Zonal Jet Migration in a 2D Quasi-Geostrophic Model

by

Ziwei Li

Submitted to the Department of Atmospheric and Oceanic Sciences,
School of Physics
in partial fulfillment of the requirements for the degree of

Bachelor of Science in Atmospheric Sciences

at the

PEKING UNIVERISTY

June 2016

Author . . . .
Department of Atmospheric and Oceanic Sciences, School of Physics
May 21, 2016

Certified by . . . .
Andrew P. Ingersoll
Professor, Division of Geological and Planetary Sciences
Thesis Supervisor

Accepted by . . . .
Yongyun Hu
Chairman, Department Committee on Graduate Theses

Zonal Jet Migration in a 2D Quasi-Geostrophic Model

by

Ziwei Li

Submitted to the Department of Atmospheric and Oceanic Sciences, School of Physics
on May 21, 2016, in partial fulfillment of the
requirements for the degree of
Bachelor of Science in Atmospheric Sciences

Abstract

In the context of studying planetary atmospheres, 2D turbulence model with parameterized moist convections (MCs) plays an important role in understanding the interaction between convections and large scale circulation. In this study, we examine the relationship between MCs and zonal jet profile. We found an important phenomenon that jets tend to "migrate" from south to north when we generate vortices with negative vorticity through a triggered scheme. Although it is found in multiple experiments [Williams, G. P., 2002], [Chemke, R. et al., 2015], it was not widely demonstrated and discussed in 2D QG system. In this thesis, we demonstrate and give an explanation on the dynamics of jet migration, and the fact that its speed is proportional to radiation strength S_r, approximately inversely proportional to β, and is also affected by Rossby deformation radius L_d. We then give an estimation of the jets' spacing via Rhines scale L_R, which is determined by L_d and parameters of moist convections. We also discussed the possible dynamical implications of L_d's influence upon migration speed.

Key Words: zonal jet migration, vortex-wave interaction, PV transport

Thesis Supervisor: Andrew P. Ingersoll
Title: Professor, Division of Geological and Planetary Sciences

准地转模型中的纬向急流迁移

李子维　大气科学

指导老师：Andrew P. Ingersoll

Abstract

在研究行星大气的领域中，应用参数化湿对流的二维准地转模式进行研究对我们理解局地对流（*Moist Convections*，*MC*）和大尺度环流的相互作用方面有着至关重要的作用。在本次研究中，我们着重探索局地对流和纬向急流形状的关系。我们发现了一个非常重要的现象：在我们持续不断地用触发的方式生成负涡度涡旋（即局地对流）时，纬向急流总是由南向北迁移。虽然有很多之前的研究也发现了这种迁移现象，但是研究者们并没有在二维准地转体系中有详细的讨论。在这篇论文中，我们提出纬向急流迁移现象并给出了动力学解释，并且给出影响迁移速率的几个变量：迁移速率正比于辐射强度 S_r，近似反比于 β，并且还受罗斯比变形半径 L_d 的影响。另外，我们用 *Rhines* 尺度 L_R 来对急流的间距进行近似，在我们的近似中，L_R 由 L_d 和局地湿对流的参数所决定。我们还进一步分析了纬向急流速度与 L_d 之间的关系所蕴含的动力学意义。

关键词：纬向急流迁移，涡-波相互作用，位涡输送

Acknowledgments

I would like to express my sincere gratitude for Professor Andrew P. Ingersoll for introducing me into the field of planetary sciences and mentoring me over this project from the summer of 2015: his advice and support have been precious from which I experienced and learned a lot. I also would like to thank Professor Yongyun Hu for monitoring me over the project as my secondary advisor at Peking University. Many thanks also to Ms. Cheng Zhang, who's always been around to support me.

Contents

List of Figures

List of Tables

Chapter 1

中文简介

一、绪论

1. 类木星大气

从组成成分来看，太阳系的行星可以大体分为两类：类地行星和类木行星。类地行星还可以被称作岩石行星，因为它们主要由金属和硅酸岩石构成。这些行星通常有坚硬的表面。另外，虽然它们的大气组成成分不同，但是厚度都比较小，通常被叫做“次生大气”。同时，这些行星更靠近太阳，太阳辐射过强，表面温度较高；并且它们的逃逸速度也较小，因此它们大气中分子质量较轻的气体在行星形成之时就逃逸了。与类地行星不同，类木行星通常有非常厚的大气层，没有坚硬的岩石表面，而且这些大气层占掉了行星的绝大部分质量。它们的质量也足够吸引轻质量的元素，包括氢气、氦气、氨气和甲烷。因为没有坚硬的岩石表面，也没有足够的太阳辐射，类木行星的大气动力结构和类地行星截然不同。这意味着我们需要用一个全新的方法来研究它们的大气。作为最大的，大气最混乱的类木行星，同时也是“类木行星”这个词的来源，木星是行星科学的一个主要研究对象。因此在这篇绪论中，我们举木星为例讨论类木星大气和类地球大气的区别。

木星和地球大气的区别主要体现在以下几个方面：1. 大气成分不同；2. 木星大气底部有一个大热源；3. 木星大气深度几乎无限，并且没有明确的边界；4. 木星半径是地球的近十倍，旋转速度是地球的两倍，这意味着科里奥利力产生的影响在木星上更加明显。从外面看地球的大气近乎透明，只吸收或者反射微量的太阳辐射，因此大气层底部的岩石表面得以升温，并且加热底层的气体使其上升。另外距离太

阳比较近也意味着不同纬度接收的太阳辐射差异更大：热带地区有能量流入，而极地地区有能量流出。因此，在地球上热带地区与极地地区的温度梯度十分明显，这样的温度梯度也是哈德雷环流、西风带、大尺度罗斯比波动的驱动力。相反的是，在木星上纬向急流非常强，并伴有巨大的湍流涡旋，而且木星大气层的厚度非常大，以至于太阳辐射不能穿透到大气层底部。木星距离太阳非常远，所以对于星球尺度的大气运动来说，太阳的短波辐射产生的纬向温度梯度几乎可以忽略不计，并且也没有和地球类似的经向环流。事实上，木星大气层顶部的气团由于红外冷却而下沉，大气层内部的气团受到内部热源加热而上升，这种结构产生的是局地对流，而不是地球上的大尺度环流。另外和大红斑一样，木星上的对流多数都是反涡旋。本次研究主要针对对流和大尺度纬向急流的相互作用，对涡旋的模拟方法也会在接下来的章节中有所介绍。

2. Inverse Energy Cascade

最新的研究表明木星的纬向急流带是由涡旋强迫的。涡旋（eddy）是流体中的一个整体旋转的结构。在木星大气中，涡旋结构通常意味着局地对流。由于二维湍流系统中的 inverse energy cascade 现象，这些局地对流会转化为纬向急流。在二维流体中，两个较小的涡旋会相互融合成为一个较大的涡旋，能量也随之从较小的尺度传递到较大尺度。如此往复，较小的涡旋持续不断地发展成为大的涡旋，而大的涡旋会相互融合成为更大的涡旋，这样能量也会从小尺度持续不断地传送到更大尺度。这和三维系统不同，因为在三维系统中，能量因为涡旋的伸展作用，从大尺度向小尺度传递。

我们以强迫-耗散系统（forced-dissipation scheme）为例简单介绍 inverse energy cascade。造成这种现象的主要原因是能量和涡度拟能（enstrophy）守恒。在一个近似无粘性的流体中，一个任意形状的涡旋在涡量空间会因为随机运动而拉长，这样它的涡度拟能会朝小尺度传递，并且它的能量会向大尺度传递（图2-1）。在强迫-耗散系统中，如果强迫（forcing）处在波数空间偏离平衡态的一个特定位置，那么就必须在大尺度内减少能量，在小尺度减少涡度拟能。这就需要系统拥有一个满足这种要求的“摩擦项”（friction）。在我们的模式中，强迫是以一个固定尺度加入的，并且大尺度能量由辐射消除，小尺度涡度拟能由耗散项消除。

3. Rhines 尺度和纬向急流的形成机理

Rhines 证明在 β 平面上，能量也存在 inverse cascade 现象：能量会从最小的涡旋尺度上升至 Rhines 尺度。在 Rhines 尺度上，流动从湍流转变为大尺度的罗斯比波动结构。Rhines 尺度由式2.3给出，其中 U 代表方均根速率。另外，由于 β 平面 x 轴和 y 轴间存在不对称性，因此 inverse cascade 在 x 轴方向会持续到 x 轴最大的长度尺度：$k_x = 0$。而在 y 轴方向则控制在 Rhines 尺度。由此，带状的纬向急流就形成了。

为什么 inverse energy cascade 会形成带状的纬向急流呢？在本次研究中我们考虑位势涡度（potential vorticity, PV）的输送特性。可逆性原则（principle of invertibility）指出，湍流涡旋带来的 PV 混合最终会产生一个现象：不同的纬度区间会被湍流运动主导，区间内的 PV 数值也大致相同，并且这些纬度区间会被 PV 梯度更大的狭小区间连接起来。这些狭小的区间水平运动以波动为主。按照这个观点，纬向平均后的 PV 场会自然地变成阶梯状的结构，这些阶梯梯度大的连接处北边就是纬向急流。

如果我们将罗斯比波动频率和涡旋周转时间（eddy turnover time）放在等式的左右两边，会得到如图2-2(a)所示像哑铃一样的 x-y 波数空间的关系。在“哑铃”内部能量的 inverse cascade 是被阻止的，但是在外部能量谱会由外向内转移到“哑铃”边界处。因此，在初始时刻是各向同性的涡旋会倾向于传递到除“哑铃”内部以外的更大尺度，向 $kx = 0$ 聚集。所以在二维准地转模式中，纬向急流可以跨过 x 方向的边界从而形成环绕整个模拟区域的纬向急流带，但是 y 方向的尺度就收到了限制而没有继续向上传送。虽然这个理论没有解释经向的急流结构尺度。但是我们有理由相信经向尺度和 Rhines 尺度是分不开的。

4. 模拟木星大气的数值方法

在对行星大气进行模拟时，我们关注其中的大尺度纬向急流，因此我们对行星大气进行简化：不可压近似、地转平衡和静力稳定条件，这些条件综合在一起就是二维准地转模式（2D Quasi- Geostrophic model, OG）。在二维准地转模式中，小尺度涡旋由于 inverse cascade 作用相互融合形成大尺度结构，当大尺度结构在 x 方向延展到边界时，纬向急流就形成了。因此我们用一个双层并且有涡旋参数化的 QG 模型对木星大气进行模拟。

我们之前的研究将木星大气分为两部分。第一部分是在外面 6bar 到 0.4bar 的天气层。天气层非常的混乱，但是也可以用肉眼分成几个不同纬度的带状区域。第二部分是有固定移动速率的深层质量源。这两层大气的边界稳定，这就需要底层的位温要低于顶层的位温。在质量源中的气体位温和天气层相同时，静力平衡被破坏，这些气体便通过湿对流交换到天气层中。与此同时，天气曾中的气体又被稳定的红外辐射所冷却，下降到底层的质量源中。因此我们引入一个触发的参数化机制。在这个机制下，对流在流函数低于某个给定下限的气旋性环流区域内被触发。这种机制的合理性在于气体被冷却的时候，气体层变薄，所以在 QG 体系中和高度正比的流函数也会相应减小。观测数据也支持这个机制。

在之前的研究中，纬向急流需要 10 年的时间来稳定下来。但是当我们再对模式进行更长时间的积分时，急流的纬向平均结构并不会长时间稳定，而是以十年际的时间尺度向北迁移。我们的结果和 [Williams, G. P., 2002]不同，在 Williams 的研究中纬向急流从两极向赤道迁移。在我们的结果中，负涡度的对流块总是从北向南移动，纬向急流也总是从南向北移动。在这篇论文中，我们从位势涡度守恒的角度给出对纬向急流迁移机制的解释。事实上，如果以下几点成立的话，迁移的现象是必然的:（1）位势涡度在整个模拟区域守恒；（2）PV 台阶保持自己的形状；（3）红外辐射对模式的强迫和湿对流强迫项抵消。我们会在接下来的章节中介绍这个结果。

我们还研究了不同的参数：β，辐射强迫 S_r，罗斯比变形半径 L_d 对迁移现象和急流间距的影响。我们发现迁移速度大体上正比于 S_r/β，并且也受 L_d 的影响。迁移速度和 S_r/β 的关系很显然，但是它和 L_d 的联系却比较复杂。在 L_d 较小的时候，MC 在台阶的平台上会停留更长的时间，只能交换较少的南北气块，而且也不能很好地转化为罗斯比波，这样就间接地影响了纬向急流的迁移速度。

在这篇论文中，第二章简单介绍了我们的 QG 模式，并分两节介绍时空分辨率和模拟区域的纵横比对模式输出结果的影响；第三章提出纬向急流的迁移现象，并分三节讨论迁移背后的动力学解释；第四章展示我们用 Rhines 尺度对纬向急流间距进行估计；最后一章我们讨论研究中出现的问题和一些有待进一步研究的问题。

二、模式简介

我们用两层准地转模式来模拟木星大气，其主要的方程如式3.1。其中 q 表示位势

涡度，ψ 表示流函数，二者成正比关系：$\psi = gh/f$。我们假定天气层的厚度为一个固定值 h_0 加上另一个高阶小量 h'，由此位势涡度可以表示为 $q = f_0 + \beta y + \nabla^2\psi - k_d^2\psi$，其中 $k_d = 1/L_d$。在应用方程3.1时，我们在其右边加上两个强迫项和一个粘性项。第一个强迫项是 S_r，表示模拟区域内相同的红外辐射强迫；第二个是触发的湿对流强迫项 $S(r,t)$。$S(r,t)$ 是场点到涡旋中心和积分时间的函数。S_r 项为正值，因此它从减小场中的流函数，代表着外界天气层的冷却效应。粘度项是 $\nu\nabla^2\zeta$，其中 $\zeta = \nabla^2\psi$。

我们用有限差分法，并加入有三对角矩阵算法的泊松模块和 x 方向的快速傅里叶变换对模式进行运算。我们用三阶 Runge-Kutta 方法对第一和第二时间节点进行初始化，然后用 Adams-Bashforth 方法计算接下来的时间步长。在每个时间步长中，我们先用上一个时间步长的物理量计算方程3.2的右边，然后在 x 方向做快速傅里叶变换，加入泊松算法内解出波数空间内的流函数 ψ，之后用傅里叶逆变换得到物理空间内的流函数。我们将 y 方向边界的流函数定为 0，来保证没有经向平均后的纬向流动，另外我们还加入 Arakawa 的雅各比架构来确保能量和涡度拟能守恒。另外我们也采用光滑的上下边界（$\zeta = 0$）。

方程3.2右边的第一项 S_r 表示辐射强迫。木星和土星的外层大气温度变化不大，因此我们将 S_r 设为正常数。第二项 $S(r,t)$ 代表着参数化对流方案。在模式中，当某场点的流函数下降到特定的下限 ψ_c 后，就会触发一个湿对流。湿对流的参数包括：成长时间 T_{mc}，半径 R_{mc}，强迫最大幅度 S_{ampl}，和下限 ψ_c。在一个实验中所有的湿对流参数都是相同的。木星的涡旋都是反气旋式，因此我们将 S_{ampl} 设为负数。

模式的两种强迫需要互相平衡来达到稳态，因此有式3.3。其中 S_{mc} 表示时间和空间平均后的湿对流强迫，C_{mc} 表示湿对流面积占总模拟区域面积的比例。我们可以由此根据 C_{mc} 和 S_r 来计算 S_{mc} 以及 S_{ampl}。S_r 的计算方法见 [Li, L. et al., 2005]，C_{mc} 等于 1×10^{-4}。

我们将默认的参数设定为：$L_d = 4000km$, $\beta = 4.26 \times 10^{-12}m^{-1}s^{-1}$, $T_{mc} = 1.7 \times 10^5 s \approx 2days$, $R_{mc} = 1000km$, $C_{mc} = 1 \times 10^{-4}$, $S_{ampl} = -3.75 \times 10^{-9}s^{-2}$, $S_r = 3.125 \times 10^{-14}s^{-2}$, $\psi_c = -1.0 \times 10^7 m^2/s$, 和 $\nu = 10^3 m^2/s$。如果不另作声明的话，这篇文章中的实验都将被设定为以上参数。默认情况的输出结果见图textcolorred3-1。

我们同样对模式的时空分辨率和模拟区域的纵横比进行了测试。在时空分辨率

的测试中，分辨率 $250km\times 250km$ 和 $125km\times 125km$ 的输出结果类似，同样时间步长在保证模式不溢出的情况下也对结果没有什么影响（见图3-2）。区域的纵横比结果见图3-3，x 轴的长度与 y 轴的长度比 α 对模式是否收敛到平稳的纬向急流结构也并没有什么显著影响。

三、纬向急流的经向迁移

在我们的实验中，纬向急流在模式启动的大概 10 年后开始形成并向北迁移（如图4-1）。在图4-1中，纬向急流在每次有一个湿对流跨越的时候都会向北“跳跃”一下。之后我们将时间分辨率调高并展示单独的一个湿对流，如图4-2(a)和4-2(b)，会发现在湿对流（MC）向南移动的同时纬向急流会在 5 天的时间内向北迁移。在图4-2(b)中，在 MC 穿过最陡的地方时，PV 台阶会先变缓，之后最陡的部分会在稍微靠北的地方重新建立起来。在这期间，MC 会将来自北边的大 PV 值气团带到南边，之后在南边和这些气团混合。这样我们提出猜想，MC 将北边大 PV 值的气团和南边小 PV 值的气团相互交换，由此导致纬向急流的迁移。

纬向急流迁移受到很多因素的影响。我们的结果有两点值得注意的地方：第一，迁移速度与辐射强迫成正相关，与 β 成负相关关系。第二，带状急流的数量随着 β 的变大而增加。因为 β 是柯氏系数 f 的一阶系数，因此这可能也是对 [Williams, G. P. et al., 1982]中旋转速率和急流个数呈正相关的结果的一个解释。

1.PV 输运

如前文所述，如果不在 β 平面上，涡旋总会将北边的气团传送到南边，将南边的气团传送到北边，这样就导致等量的南北 PV 输运。但是模式是建立在 β 平面上的，在 MC 将北部气团传送到南边时，MC 本身也会向南边运动，因此它们会将这些气团“推”向更南边；与此同时被传送到北边的南部气团就会保持他们传送后的位置。因为通常来说北边气团的 PV 值要大于南边气团，因此综合来看 MC 会将南北气团对调，然后将原先北部的气团带到更南边，并在那里与之混合。

关于 PV 传送的更详细讨论在英文版正文的第三章第一节。

2.PV 台阶

由于我们的参数化设定，MC 生成于模拟场的最低处，一般在它所要经过的急

流带的北边。同时也在 PV 台阶最陡的地方 BC 的北边（见图4-4(a) 和 4-4(b)）。当 MC 发生在台阶的平面 AB 上时，它会向南移动并经过两平台连接处 BC，然后在 AB 下面的第二个平台 CD 上消失。由于 PV 传送效应，AB 的一部分 PV 值较大的气团被 CD 的 PV 值较小的气团取代，这也可以理解为对罗斯比波动的一次扰动。较大 PV 值的气团在 CD 上和 MC 混合并消失。因此，虽然看起来 MC“减小”了 BC 的 PV 值，但这实际上是 PV 传送和混合的结果。

正常来说一个时间段内会有很多 MC 产生，在它们每次穿过急流带时都会迫使急流带向北移动，这样造成场内的急流带整体持续不断地向北迁移。MC 对 PV 的负强迫与辐射的正强迫相互平衡，更确切地说是辐射的负强迫迫使 MC 进行正强迫，使得模拟场内 PV 守恒。虽然 MC 是造成急流迁移的动力，但是我们假设：单独的 MC 并不会对整体急流结构，同时也是 PV 台阶，的形状产生很大影响。因此虽然持续不断地受 MC 影响，但是 PV 台阶的形状从模式平衡到稳定的纬向急流后就保持不变。在 y-PV 平面内，由红外辐射的作用，PV 台阶在 PV 轴向上移动；由于 MC 对 PV 的输运作用，PV 台阶在 y 轴向北移动。因此，PV 台阶保持相同的周期形状，从左下向右上边移动。

3. 迁移速度

在这部分我们将介绍迁移速度与 S_r/β 的关系，以及它与 L_d 的关系。根据 PV 的表达式，在 y-PV 平面中 PV 的基准斜率是 β。从图4-5(a)可知迁移速率与 S_r 呈正相关，与 β 成负相关。在 y-PV 平面中，由于辐射强迫和 MC 强迫分别使得 PV 台阶向上和向右移动，因此总的迁移速度矢量应该是沿着斜率为 β 的直线向右上方。因此我们在物理空间中看到的迁移速率应该是这个矢量在 y-PV 平面 y 轴上面的投影。因此我们引入一个迁移速率的预测量 $u_{mig} = S_r/\beta$。不过迁移速率并不是简单地正比于 β 的倒数，而且它还受到由 L_d 控制的罗斯比波数的影响。这些影响体现在以下两方面：（1）PV 台阶的平台斜率会受到不同 β 的影响；（2）小尺度湍流和大尺度波动之间的转化效率，同时这种效率受到 L_d 和 R_{mc} 的影响。

第一．根据图4-6，PV 台阶上面的平台并不是水平的：它的斜率受制于 β 的取值，因为更大的 β 意味着更倾斜的 PV 平面。因此，当 MC 穿过一个纬向急流带时，它会迫使 PV 台阶上连接两个台阶的部分沿着台阶平面的斜率向右上方移动。因此 MC 造成的 PV 台阶移动就会沿着平面斜率向右上方，而不仅仅是右方了。在

这个条件下，如果给定台阶平面的斜率 k'，那么实际迁移速率为 $u'_{mig} = S_r/(\beta - k')$。

第二，迁移速率与罗斯比变形半径成正相关，如图C-2。在我们的结果中，L_d 小的时候罗斯比波动的传播速度要小于 L_d 大的时候。并且 L_d 小的时候，MC 在 y 方向的速度要小一些，因此它将北边的大 PV 空气团传递到南方的作用就没有 L_d 大的时候明显，它们从北向南跨越的急流数目也有所减少，交换的 PV 也会少一些。

另外，L_d 与迁移速度的关系或许隐含着在更重要的意义。在二维湍流地球流体中，大尺度纬向急流由小尺度湍流向大尺度波动扩展的 inverse cascade 得到，并且湍流和波动的交界尺度由 Rhines scale 给出。但是我们并不知道湍流尺度以什么样的速率扩展到波动尺度。在我们的结果中，罗斯比波数随着 L_d 的增加而减少，也就是说罗斯比波长随着 L_d 的增加而增加，我们因此给出一个波长尺度 λ。在图C-2和图4-5(a)所代表的实验中，λ 随着 L_d 的增加而逐渐接近 R_{mc}，并且迁移速度也逐渐增加。这就引出了我们对迁移速率的另外一个解释：当 λ 接近涡旋的尺度时，涡旋能够效率更高地将能量转化为罗斯比波动，同时将自己的负涡度融入 PV 台阶的 BC 段中。这样迁移速率就会得到增强。如果这个解释成立的话，迁移速率就可以指代 MC 和大尺度波动结构的相互作用的速率。另一方面，罗斯比波长尺度看起来 λ 也受到 L_d 的影响，这需要进一步实验的证明。当然这个尺度 λ 同样也可能与 Rhines 尺度相联系。

四、急流的间距

在我们的实验中，急流总是从南边的边界产生，从北边的边界消失。纬向急流迁移的形态是等间距，有周期性并且固定的，所以我们可以用统计分析的方法对平均后的急流的间距进行分析。我们分析的方法是先对纬向平均后的急流进行光滑化，然后计算每个时间步长的波峰和波谷的距离平均值和标准差。计算后的结果见图5-1(a)。在其他变量相同的情况下，L_d 较大时急流个数较少，间距较大。

根据绪论部分的第四章，由于 β 平面的各向异性，x 方向（纬向）的尺度远大于与 y 方向（经向）的尺度，但是经向尺度和 Rhines 尺度成正比。我们发现罗斯比变形半径 L_d 和单个 MC 的总强迫 S_{int} 与急流间距有关。S_{int} 的表达式见英文版第四章。

我们用 Rhines 尺度来估计纬向急流间距。Rhines 尺度由：$L_R = \sqrt{\frac{U}{\beta}}$ 给出，其中 U 由式5.2估计。这样 Rhines 尺度的表达式为式5.3。在式5.3中，当 L_d 减小时，

纬向急流间距增加。另外它还与湿对流半径 R_{mc} 负相关，和单个 MC 的总强迫 S_{int} 正相关。图5-1(b)表示 L_R 可以很好地预测纬向急流的间距。

五、结论和展望

这篇论文讨论了我们模式中用到的木星大气和二维准地转流体的理论背景，并且对模式的框架进行了简单介绍。之后我们详细提出，解释并讨论了我们模式中出现的年代际纬向急流迁移的现象。

在木星的二维湍流系统中，辐射的能量需要和湿对流能量平衡，同样位势涡度也应该互相平衡。在 y-PV 平面中，辐射使得 PV 台阶向上移动，MC 对空气团的输运和混合作用使得台阶向右移动。因此由于辐射和湿对流的相互平衡，纬向急流迁移是一个必然现象。根据这个猜想，我们引入 $u_{mig} = S_r/\beta$ 并发现实际的迁移速度与之相近。这证明了我们对于用 PV 输运解释急流迁移的猜想是正确的。我们还解释了为什么 β 和 L_d 会导致实际的迁移速率与 u_{mig} 不一致。

另外，L_d 会影响迁移速率的这个事实可能还隐藏着一些湿对流与纬向急流相互作用的动力学过程。在我们的结果中，湿对流（涡旋）会各向异性地从有限的小尺度发展成为 y 方向和 Rhines 尺度相似的尺度和 x 方向几乎无限的尺度；但与此同时也在 x 方向展现了另一个一个特定的尺度。在 x 方向的罗斯比波动解并没有限制波长，但是我们的结果却有一个受限于 L_d 的波长尺度 λ。这个尺度对于涡旋波动相互作用有着决定性的影响：MC 的尺度越接近 λ，就会越容易被吸收并转化为罗斯比波动能量。

以上的讨论也提出了若干有待于解决的问题：

（1）模式中固定的罗斯比波长是有什么决定的？在我们的结果中它看起来受制于 L_d，但是它也是在涡旋转化为波动时产生的。因此一定有未发现的动力作用隐藏其中。

（2）在纬向上，λ 尺度和 Rhines 是一致的吗？Rhines 尺度可以理解为表示经向的急流间距，但是在 x 方向却没有与之对应的尺度。在另一方面，如前文所述罗斯比波长的行为却和 Rhines 尺度非常相似。因此 λ 可能是 Rhines 尺度体现在 x 方向的一个形式。

（3）木星上真的有纬向急流迁移现象存在吗？我们的实验表明，纬向急流迁移的速率大概在 $10^{-2} m/s$ 的尺度上，因此通过现有的数据我们可能没有办法观测到

这样的现象。但是到底这个现象存在与否，深入地研究纬向急流的行为将有助于我们理解二维准地转湍流体系的性质。

Chapter 2

Introduction

2.1 Jovian Atmospheres

In terms of composition, solar system planets are roughly divided into two major categories: Terrestrial planets (Mercury, Venus, Earth and Mars) and Jovian planets (Jupiter, Saturn, Uranus, and Neptune). Terrestrial planets are also referred to as rocky planets because they are primarily composed of metals and silicate rocks. These planets have solid surfaces (or some has liquid surface such as Earth) and although made of different primary components such as nitrogen (Earth), carbon dioxide (Venus and Mars), their atmospheres are relatively thin, referred to as secondary atmospheres. For warmer inner terrestrial planets, most of its light gases during its formation is lost due to hot surface temperature because of too much solar radiation, small mass of the atoms and insufficient escape velocity of the planet. Different from Terrestrial planets, Jovian planets have tremendously thick atmospheres which take up most of their masses, and they don't have solid surface. They are massive enough to attract and hold large quantities of light elements. They are also called the outer planets because they are further than the inner planets, resulting in much less intake of solar radiation. Jovian atmospheres are primary atmospheres composed of mostly light gases as hydrogen, helium, methane, and ammonia [Taylor, F. W., 2010].

Because of no obvious rocky surfaces and considerate energy intake from the sun, Jovian planets (also called gas giants) have completely different dynamics regime from terrestrial planets like the earth. This posed a problem which should be dealt with in a novel approach. As the largest and most turbulent jovian planet in the solar system, also where the word "Jovian" adapts from, Jupiter serves as a primary example in the field of planetary atmospheres. We thus take Jupiter as an example to show differences between terrestrial atmospheres and jovian atmospheres in this introductory section.

There are several predominant differences between Jupiter's and Earth's atmospheres: 1. difference in atmospheric composition (hydrogen, helium, methane and ammonia in Jupiter and nitrogen, oxygen, water vapor and carbon dioxide); 2.a large heat source beneath Jupiter's atmosphere; 3. essentially infinite depth of Jupiter's atmosphere without solid wall lower boundary, which indicates that there is no constraint on vertical movement or frictional drag; 4. jupiter's ten times' diameter and more than two times' rotation rate compared with earth, which means that the Coriolis force on Jupiter is much larger.

From the outside, the earth has transparent atmospheres that absorbs or reflects little solar radiation, which allows the rocky surface beneath to heat up, warming air parcels near the surface to ascend. And being near to the sun also means solar radiation is more strongly affected by latitudes: positive net influx in the tropics and negative influx in the polar areas. Thus the temperature gradient between tropical zones and polar regions is apparent on earth, which forces the Hadley circulation, westerlies and Rossby wave. On the other hand, Jupiter has very strong zonal jets together with giant turbulent eddies, and it has extremely thick atmosphere which makes itself impenetrable by the solar radiation. Distant from the sun, Jupiter also intakes negligible short wave energy. Thus it has negligible latitudinal temperature gradient in view of global scale atmospheric movements, and it has no global meridional circulation as the earth. Instead, upper air parcels are cooled because of outgoing infrared radiation, and inner air parcels are heated by internal hear source. This scheme results in only regional convection, unlike the general circulation on earth. Convections on Jupiter are almost anti-cyclonic, the great red spot being the primary example. This study mainly focuses on the interaction between convections and large scale zonal jet structures, and our treatment will be discussed in the latter parts.

2.2 Inverse Energy Cascade

Current researchers hypothesised that the jet bands on Jupiter, highly turbulent in small scale but constant in global scale, is driven by eddies. An eddy is a region in the fluid that is behaving coherently and rotationally. In terms of Jupiter's atmosphere, eddy largely means regional convections. These regional convections are transformed into strong zonal jets because of the Inverse Energy Cascade in 2D turbulence system. In 2D fluids, vortices (convections) interact with each other by way of ”vortex cannibalization”, when two small eddies merge into one larger eddy, and energy flows from small to larger length scales. In the scheme of 2D Inverse Energy Cascade, energy from smaller scale is expected to consecutively cannibalizes into larger length scales, which means that initial small eddies tend to cluster and merge into larger eddies, and larger eddies are also expected to create even larger eddies [Rivera, M. K., 2000]. It is quite different from 3D system because in 3D systems, energy flows from large to small length scale due to eddy stretching.

We will describe briefly about the inverse energy cascade in the forced dissipation scheme of 2D turbulence system. The counter intuitive behaviour of inverse cascade is due largely to the interacting conservation of energy and enstrophy [Vallis, G. K., 2006]. The enstrophy is defined as equation 2.1

$$Z = \frac{1}{2}\int_A \zeta^2 \mathrm{d}A. \tag{2.1}$$

In a nearly inviscid fluid, a vortex of any shape would be elongated due to stochastic motion of fluid, and because the area of vortex is preserved, the vortex would appear tilted. At the same time, the enstrophy is moved to smaller scales while energy is moved to larger scales (figure 2-1). In the forced dissipation scheme, where forcing scale is usually at a separated set of scales in the spectrum space, the energy must be removed at larger scales while enstrophy must be removed at smaller scales. This requires that in order to acquire a steady state, the modelled system must have such friction that satisfies this removal requirement. In our model, forcing is added with stirring of one constant scale, and the transferred large-scale energy is reduced by uniform radiation forcing, and small scale enstrophy is balanced by dissipation.

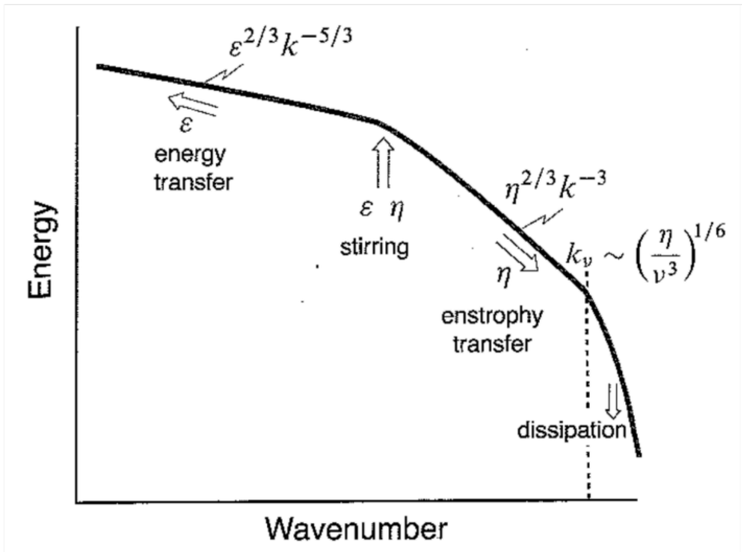

Figure 2-1: Energy spectrum of the 2D forced-dissipative turbulence system. Energy and anstrophy are injected in form of "stirring" at a particular scale. Then energy is transferred into larger scales (smaller wave numbers), whereas anstrophy is moved to smaller scales (larger wave numbers) and then dissipated at that scale.

As for Jupiter, the shallow layer are seen as a 2D turbulence system because of its large horizontal scale and small vertical scale. According to [Williams, G., 1978] the primary hypothesis is made that Jovian characteristics–the axisymmetry and scale of the bands, the zonal currents, the waves and eddies–are all essentially a feature of two dimensional turbulence on a rapidly rotating planet, with the turbulence being energised by baroclinic instability. The consistently produced moist convections served as continuous replenishments for the Inverse Energy Cascade. Therefore, moist convections serve as small eddies that merge together into larger eddies, and when a large eddy stretches onto the boundaries in x direction, it becomes large scale zonal jet structure.

2.3 The Rhines Scale and Zonal Jet Formation

Rhines [Rhines, P. B., 1975] showed that on a β plane, there is an inverse cascade in energy spectrum. The inverse energy cascade ranges from scales from the smallest turbulence scale up to the Rhine's scale. At Rhine's scale, the flow motion turns from turbulence to large scale Rossby wave regime. Consider geostrophic turbulence that is stably stratified and in near-geostrophic balance, we have equation:

$$\frac{\partial \zeta}{\partial t} + \mathbf{u} \cdot \nabla \zeta + \beta v = 0. \tag{2.2}$$

If $\zeta \sim U/L$ and $t \sim T$, then all three terms in the equation is scaled as $U/(LT)$, U^2/T, and βU. The time-dependent term is determined by the other two terms, in other word, time scales associated with advection or Rossby frequency is determined by length scale. If scale L is small, advective term dominates representing eddy advection and mixing, and if L is large, the β-term is dominant, which represents Rossby wave propagation. The cross-over scale is therefore given by

$$L_R = \sqrt{\frac{U}{\beta}}. \tag{2.3}$$

The U represents root mean square velocity which is easier to evaluate, though might not be satisfactory in view of turbulence. In fact when we really look into the cross-over scale using phenomenology of two-dimensional turbulence, equating eddy-turnover time $\tau_k = \epsilon^{-1/3} k^{-2/3}$ and inverse Rossby wave frequency k/β we have the β-scale

$$L_\beta = \left(\frac{\epsilon}{\beta^3}\right)^{1/5}, \tag{2.4}$$

where ϵ means energy input per unit volume by stirring. However, the scales, L_R and L_β, are not necessarily energy containing scale, but just the scales at which β term in the vorticity equation becomes dominant: inverse cascade can continue to transform energy to larger scales [Vallis, G. K., 2006]. The inverse energy cascade thus is not "suppressed" at Rhines scale, or β scale. In the context of geophysical turbulence on a β plane, there is, however, an asymmetry between x direction and y direction that inverse cascade continues to $k_x = 0$, which is the largest scale possible in x direction, while remaining constrained to the Rhines scale in the y direction. Therefore the banded zonal jet structure is formed.

To explain how inverse energy cascade is transformed into formation of banded zonal jet structure, we need to focus on the advective characteristic of potential vorticity (PV). The principle of invertibility suggests that PV mixing by turbulent eddies would eventually result in distinct latitudinal regions dominated by horizontal vortical motions where the PV is almost homogenized, separated by sharper jumps of PV on which the motion has a more wavelike character. According to this view, the zonal mean PV field develops naturally into a staircase structure; the flow is anisotropic and typically dominated by narrow zonal jets along the jumps in PV [Scott, R. K. et al., 2007]. The wavelike sharp separations between each PV regions is where Rossby wave dominates.

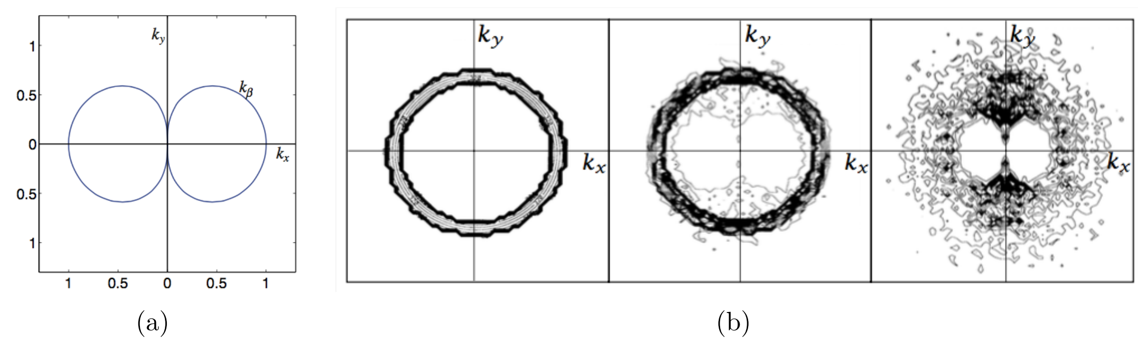

Figure 2-2: (a) The anisotropic boundary between turbulence and Rossby wave. Out of the "dumbbell" like boundary, turbulence term dominates, and energy spectrum can cascade from smaller scale to larger scale, while inside the dumbbells, wave like structure dominates and energy transfer is suppressed. (b) Free evolvement of an eddy's phase space on a beta plane. The eddy is initialized to be isotropic, but later piled up near $k_x = 0$ and excluded the dumbbell area, which means that the eddy's latitudinal length scale dominates over its meridional length scale.

Here is a simple explanation of how cascaded large scale results in banded zonal jet structure. There is anisotropy inherited in Rossby wave, and such anisotropy can give rise to predominantly zonal flows and jets [Vallis, G. K., 2006]. We assume that the turbulent eddy transfer rate is inefficient at the scales we are discussing, and Rossby wave dominates the dynamics. If we equate the Rossby wave frequency and the inverse of eddy turnover time, we have solutions for x and y wave number components in a dumbbell like shape (see figure 2-2(a)).

Within the dumbbell energy cascade is inhibited while out of the dumbbell, the energy spectrum will transform onto the dumbbell boundary. Therefore, if evolves freely (figure 2-2(b)), an initially isotropic spectrum would cascade into larger scales but avoiding region inside the dumbbell and piling up where $k_x = 0$ [Vallis, G. K. et al., 1993]. Therefore banded jet structure is formed across the x boundary, resulting in banded zonal jet structures, while on the other hand, meridional structure remain constrained from cascading to larger scale. The meridional jet structure is not clearly explained in this simple theory, but we can expect the meridional wave number to be closely, if not precisely, associated with the β or Rhines scale.

2.4 Numerical Modelling Approach to Jupiter's Atmosphere

In numerical simulation of planetary atmospheres, we focus on its large-scale and often complex zonal jets. We introduce incompressible flow, geostrophic balance and hydrostatic condition, which lead to the so called Quasi-Geostrophic model. In 2D Quasi-Geostrophic(QG) system, eddies merge together into large structure because of the inverse energy cascade, and when the large structure stretches across zonal boundaries, jets are formed. Thus we use a 2-layered QG model to simulate planetary zonal jets by generating eddies, which represent moist convections.

According to our preliminary investigation [Li, L. et al., 2005], Jupiter's atmosphere is divided as follows. One is shallow weather layer on the outside, which is between the base of the water cloud at ~ 6 bars and the level of emission to space at ~ 0.4 bars. It is also highly turbulent and can visibly segregated into several bands at different latitudes. The other is a deep reservoir with constant movement, with a stable interface between itself and the weather layer. This scheme is stable if weather layer has potential temperature higher than the reservoir. Air parcels from the reservoir is converted into the weather layer when its potential temperature equals to that of the weather layer, and its hydrostatic balance is violated, and a regional moist convection event is produced. At the same time, steady infrared radiative cooling converts the weather layer air parcels into the deep reservoir. We therefore introduce a triggered parameterisation of convection, in which convections are triggered in cyclonic regions in the upper layer, where the stream function falls below a threshold. This is reasonable because when air parcels are cooled, their layer depth becomes shallow, and so does the stream function because they are proportional to each other in a QG system. This treatment fits also into observations [Little, B. et al., 1999].

When air parcels are injected from deep reservoir into the weather layer, mesoscale anticyclones are generated, with negative vorticity forced into the domain. The steady radiative cooling effect generates positive vorticity. This scheme serves as a balance between anticyclonic and cyclonic forcing which satisfies conservation of PV. During the adjustment between small-scale turbulence and large scale radiation forcing, the energy injected by MCs are transformed to large scale structures like the Great Red Spot and zonal jets via inverse energy cascade [Li, L. et al., 2005]. And the mechanical energy is conserved with small scale turbulence energy injection and large scale dissipation [Scott, R. K. et al., 2007].

It generally takes a short time (about 10 years) for zonal jets to stabilize, but when we integrate for a longer time, the jets' profile does not maintain stable but is migrating in decadal scale. We found our result different from that obtained by [Williams, G. P., 2002], where jet migrates to the equator. In our model, negative MCs tend to move from north to south, and zonal jet structure almost certainly moves from south to north, which seems not quite physical. In this thesis, we give an explanation in terms of the conservation of potential vorticity (PV). In fact, this migration must happen if: (1) conservation of PV retains all over the domain; (2) PV staircase profile maintains; (3) radiation forcing is balanced by moist convection forcing. We will demonstrate this result In the later part of this article.

We also examined different parameters: β, radiation forcing S_r, deformation radius

L_d and their effects upon the migration phenomenon and jets' spacing. We found that the migration speed is roughly proportional to S_r/β, and is also affected by L_d. The relationship between migration speed and S_r/β is obvious. But it is rather complicated between migration speed and L_d, because L_d affects the MCs' movement by controlling time that MC stays in one staircase plane, in that under condition of smaller L_d, MC stays on the platform for longer time, exchanging less air parcels between north and south, and is harder to transfer into Rossby waves compared with larger L_d.

In this thesis, the second chapter gives a short description about our QG model, and is composed of two sections discussing time, spatial resolution and aspect ratio's impact upon the model output; the third chapter introduces the meridional migration found in our results, and is composed of three sections discussing a possible explanation of the dynamics underlying jet migration; the fourth chapter shows our prediction of jets spacing by calculating the Rhines scale L_R; the last chapter discusses problems in our research and leaves some open questions awaiting further investigations.

Chapter 3

Model Description

We simulate gas giant's atmosphere with a two-layer Quasi-Geostrophic model. We set the deeper layer as the reservoir, and the other layer as the weather layer. The primary equation is as follows:

$$\frac{\partial q}{\partial t} + J(\psi, q) = S_r + S(r,t) + \nu \nabla^2 \zeta \tag{3.1}$$

q denotes potential vorticity (PV), ψ denotes stream function, and it's proportional with layer depth h by $\psi = gh/f$. In our model's approximation, we assume layer depth $h = h_0 + h'$, and $h' \ll h_0$. We run the model on β plane, so that $q = f_0 + \beta y + \nabla^2 \psi - k_d^2 \psi$, which is to the first accuracy, where $k_d = 1/L_d$, L_d being the Rossby deformation radius.

While adapting equation 3.1, we have two forcing terms and one viscosity term to its right-hand side. One of the forcing is uniform radiation S_r, which is the same constant all over the domain, and the other forcing term is $S(r,t)$, which is triggered by a threshold value ψ_c. $S(r,t)$ is dependent on the field point's distance to the convection center and integration time. The uniform radiation term S_r is positive so it reduces ψ off the domain, and represent cooling effect on the outer layer. The viscosity term is $\nu \nabla^2 \zeta$, where $\zeta = \nabla^2 \psi$. And the equation is changed to 3.2:

$$(\nabla^2 - k_d^2)\frac{\partial \psi}{\partial t} + J(\psi, g) = S_r + S(r,t) + \nu \nabla^2 \zeta. \tag{3.2}$$

In this equation, g is given by $g = \zeta - \beta y + \psi_2$ and the ψ_2 is the stream function of the deeper layer, acting as a reservoir. This value, ψ_2 should be used later when we discuss uniform under flow.

We use finite difference scheme with a Poisson module containing a tridiagonal matrix solver and Fast Fourier Transform module from the Numerical Recipes [Press, W. H. et al., 1986] to solve equation 3.2. The model is initiated via Runge-Kutta third order algorithm for the first and second time step, and then integrates in Adams-Bashforth scheme. In every time step, we evaluate the Jacobian term, viscosity term and triggered convection adjustment using the values from previous time step. Then we feed the adjusted time derivative of ψ and the right-hand side of equation 3.2 into the Poisson solver, which performs Fourier transform along the x axis first, solve the tridiagonal equation in the frequency space, and then perform reverse Fourier transformation to get stream function in the physical world. We set the initial field's two boundaries in y axis $\psi = 0$, and $\frac{\partial \psi}{\partial t} = 0$ in every time step, to secure stream function being the same on the two boundaries, to maintain no mean zonal flow. And we adapt Arakawa's Jacobian boundary regime to satisfy conservation of energy and enstrophy in space [Arakawa, A., 1966]. We also create stress-free boundary by setting $\zeta = 0$ on the boundaries.

The first term on the right-hand side of equation 3.2, S_r represents radiation. As Jupiter and Saturn have almost uniform temperature of the outer layer, we set term S_r constant and positive. The second term $S(r, t)$ represents our parameterization treatment towards convection. We set certain threshold value of stream function as ψ_c, once the stream function of one particular region in the domain falls below ψ_c, one convection will be triggered. Moist convections (MC) have parameters as age T_{mc}, radius R_{mc}, forcing amplitude S_{ampl}, and triggering value ψ_c. In one experiment, all of the convections have the same T_{mc}, R_{mc}, and S_{ampl}. And their forcing varies as time develops in a parabolic form: $t(T_{mc} - t)$ after it is created. Also we set S_{ampl} negative to create anticyclonic convections. These anticyclonic convections simulates hotter air injecting from deep layer into the upper layer. In order to meet mass conservation, the radiative forcing and MC forcing should balance each other, therefore we introduce equation 3.3:

$$S_r + S_{mc} \times C_{mc} = 0 \tag{3.3}$$

Where S_{mc} is given by:

$$S_{mc} = \frac{1}{T_{mc}} \frac{1}{\pi R_{mc}^2} \int_0^{T_{mc}} \int_0^{R_{mc}} S(t, r) 2\pi r dr dt \tag{3.4}$$

and $S(r, t) = S_{ampl}(1 - \frac{t}{T_{mc}})\frac{t}{T_{mc}}(1 - \frac{r^2}{R_{mc}^2})$. so $S_{mc} = \frac{1}{12} S_{ampl}$. Different from S_{ampl} and $S(r, t)$, we have S_{mc} representing the time and space averaged forcing produced by MCs. C_{mc} is the fractional area of MC over the global disk. Because we assume that positive PV forcing is balanced by negative PV forcing, we can use this as a parameter to evaluate S_{mc} given S_r [Li, L. et al., 2005]. C_{mc} is set to 1×10^{-4} based on Galileo [Little, B. et al., 1999] and Cassini [Dyudina, U.A. et al., 2004] observations. S_r is evaluated under the conservation of mass, see the Appendix A in [Li, L. et al., 2005].

We set our default parameters as: $L_d = 4000km$, $\beta = 4.26 \times 10^{-12} m^{-1} s^{-1}$, $T_{mc} = 1.7 \times 10^5 s \approx 2days$, $R_{mc} = 1000km$, $C_{mc} = 1 \times 10^{-4}$, $S_{ampl} = -3.75 \times 10^{-9} s^{-2}$, $S_r = 3.125 \times 10^{-14} s^{-2}$, $\psi_c = -1.0 \times 10^7 m^2/s$, and $\nu = 10^3 m^2/s$. Unless otherwise epecified, experiments in this thesis are fixed with the same parameters as above. The default output result is shown in figure 3-1.

3.1 Resolution

We tested two spacial resolutions, $250km \times 250km$ and $125km \times 125km$, and three lengths of time steps to find out the difference. The parameters and results are shown in table 3.1 and figure 3-2

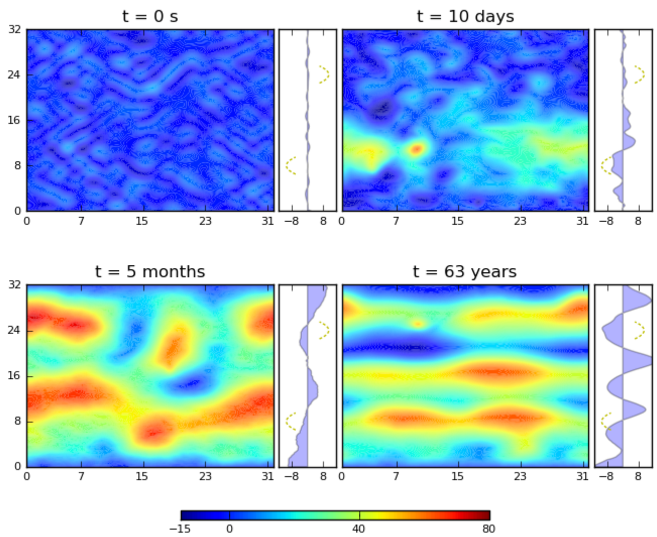

Figure 3-1: Standard output of the model. These figures correspond to different stages: the upper left is the initial pattern; the upper right is integrated for 10 days; the lower left is 5 months and lower right is 63 years, when the model converges to a steady pattern of zonal jets. Within each panel, contour graph on the left is stream function ψ in $10^6 m^2/s$, with x and y ticks in $1000km$; and the profile figure on the right is zonally averaged velocity, in terms of $1m/s$. The yellow dashed lines in each plot are defined by $d^2U/dy^2 = \beta$.

label	resolution(km)	time step($10^3 s$)
(a)	250×250	1.0
(b)	250×250	0.5
(c)	125×125	1.0
(d)	125×125	0.5
(e)	125×125	2.0

Table 3.1: resolution test parameters

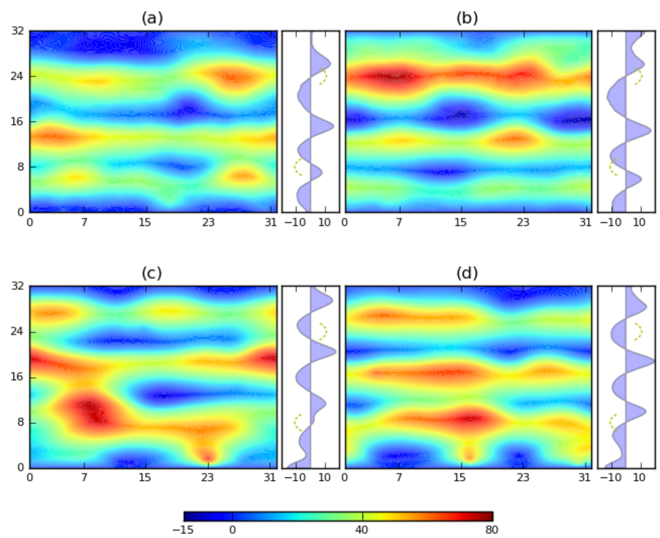

Figure 3-2: The plot of resolution experiments. (a) and (b) corresponds to time step $1.0 \times 10^3 s$ and $0.5 \times 10^3 s$, with spatial resolution of $250km \times 250km$. (c) and (d) corresponds to time step $1.0 \times 10^3 s$ and $0.5 \times 10^3 s$, with spatial resolution of $125km \times 125km$. All the snapshot are taken at the time step for $7.5 \times 10^8 s$, which is 23.8 years.

Our model failed to produce converged result in case (e) when time step is set to $2.0 \times 10^3 s$ when resolution is $125km \times 125km$. And except this, spatial and time resolution does not have significant effect on the stream function field and zonal velocity profile. Thus we set spatial resolution as $250km \times 250km$ and time step $1.0 \times 10^3 s$ as our default parameter.

3.2 Aspect ratio

In this section, we would like to examine the results of setting different lengths of x boundary, while keeping y boundary length the same. The parameters is written in table 3.2.

Table 3.2: aspect ratio test parameters

aspect ratio($X \times Y$)	domain($10^3 km$)
128×129	32×32
256×129	64×32
512×129	128×32

We found that when x axis is extended, KE_{zonal}/KE_{eddy} becomes smaller. KE_{eddy} denotes eddy kinetic energy, and KE_{zonal} denotes zonal mean kinetic energy. KE_{eddy} and KE_{zonal} is defined by:

$$KE_{eddy} = \sum_{i}^{LenX} \sum_{j}^{LenY} \frac{1}{2}(u'^2_{i,j} + v'^2_{i,j}), \tag{3.5}$$

$$KE_{zonal} = \sum_{j}^{LenX} \sum_{i}^{LenY} \frac{1}{2}(\overline{u_j})^2, \tag{3.6}$$

where $u' = u - \overline{u}$, $v' = v - \overline{u}$ (the over line means zonal average). In our program, $\overline{v}$ equals to zero because we adapt solid wall boundary in y axis. If the ratio $\alpha = KE_{eddy}/KE_{zonal}$ is small, it means that we have better zonal jets structure, and if it's large, then eddies dominate the whole domain. On the other hand, longer x axis means that if we do experiments on a region more like a "band" on the planet rather than a square "region" on the planet. As illustrated in figure 3-3, the aspect ratio doesn't affect zonal velocity profiles very much. Each peak-like anomaly in figure 3-3 reflects one triggered MC event. When integrated time goes to more than 15 years, α in all three experiments remain under 0.5, while as x boundary prolongs, the peaks are smoother in the profile. It is true because we use the same parameters of

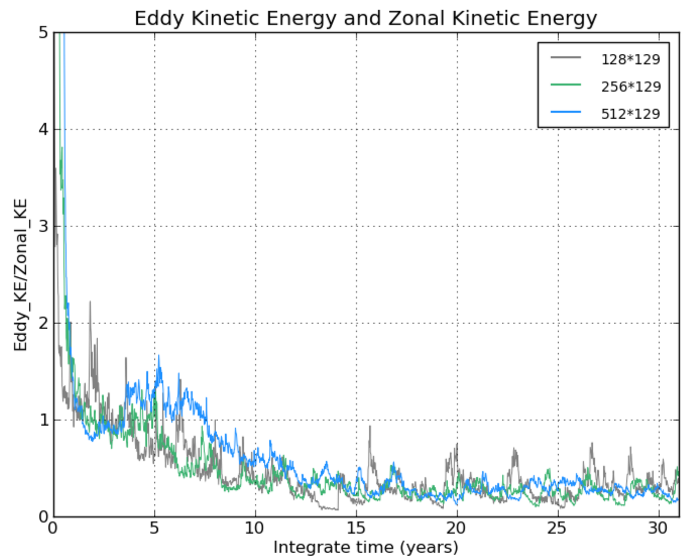

Figure 3-3: Ratio of eddy kinetic energy to zonal mean kinetic energy. All the three experiments are integrated for 10^6 steps, which is 10^9 seconds, approximately 31.71 years.

convective events, larger domain (longer x axis) means MCs happen more frequently, but at the same time, during each MC event, there are more banded jet structures compared with vortex structures. Therefore when x boundary is long, α becomes smoother but comes with more anomalies. However, since 128×129 grid points already have acceptable α values, we use grid points 128×129 as default aspect ratio unless otherwise specified.

Chapter 4

Meridional Migration of Zonal Jets

In this chapter, we first show the result in our default run that zonal jet migrates after the model converges from small-scale eddy turbulence scheme to a large-scale and stable zonal jet structure. Then we further discuss the mechanism and properties of jet migration in terms of eddy momentum flux and PV transportation of MC, PV mixing and PV staircase associated with zonal averaged jet structure, and migration speed as a confirmation of our hypothesis.

In our experiments, jet starts to migrate in about a decade after the model is initiated. This phenomenon is clearly demonstrated in figure 4-1. The zonally averaged jet profile remains almost the same as they moves from south to north.

From figure 4-1, it is shown that zonal jets ”jump” as one convective event happens, and we increase the time resolution, and track one convective event, as in figure 4-2(a) and figure 4-2(b). From figure 4-2(a) we can see that as one single MC moves to the south, zonal jet moves from south to north in a short time scale, about 5 days. This is why in figure 4-1, jet structures appear to be discrete components that ”jump” northwards as MC goes across when expressed in years' scale. In figure 4-2(b), PV staircase is smoothed and pushed northwards when MC goes across the steepest part, and then the steepest part reforms a short distance north of its original place, during which MC carries large PV air parcels from the north to south and then mix with them in the southern flat region. This coincides with our hypothesis of PV transportation that during an MC event, larger PV in the north is transported to

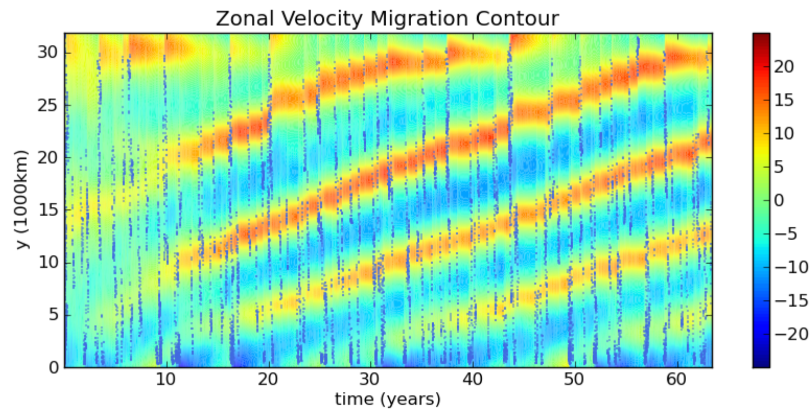

Figure 4-1: Hovmoller diagram of velocity field (m/s), representing zonal jet migration. In this diagram, y axis is meridional coordinate in terms of $1000km$, and x axis is time, in terms of years. The blue tiny dots on this figure is MC tracks. Zonal jets migrate as MCs cross the banded jet streams, while it is stable in time intervals between MC events.

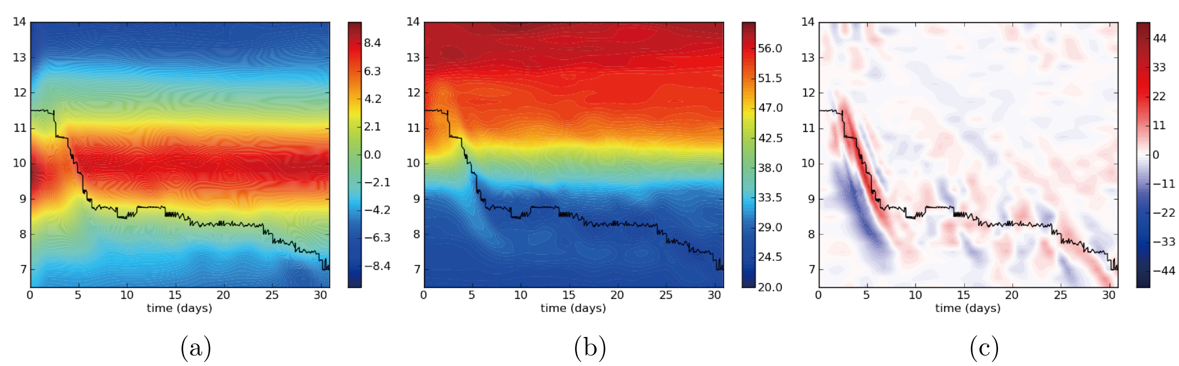

Figure 4-2: Contour plot of (a) zonally averaged velocity (m/s) and (b) PV ($10^{-6}s^{-1}$) during a MC event. The black track is MC center's y coordinate plot with time. In this diagram, y axis is meridional coordinate in terms of $1000km$, and x axis is days. Figure (a) shows that when MC crosses a zonal jet band, it moves the local maxima of zonal averaged velocity to the north, in days' scale. Figure (b) demonstrates the PV transport scheme of the MC vortex: in the first several days, MC accumulates with time by S_{ampl} forcing; after day 5, it moves southwards together with parcels of large PV south of it, while continue mixing with these parcels; at the same time, albeit hard to recognise, the steepest part of PV (say, the center of the yellow band) is moved northward by about $100km$. Figure (c) shows PV zonal averaged transport. There is a strong positive PV transport surrounds MC while a strong negative PV transport is south of it, representing MC's southward movement of itself and its surrounding PV transport respectively.

south while smaller southern PV is transported to the north.

The zonal jet migration structure is affected by various parameters. Our results have two noticeable properties. First, the migration speed has a positive correlation with radiation forcing and negative correlation with β. The fact that β decrease migration speed could be interpreted as an increase with rotation rate, which coincides with [Chemke, R. et al., 2015]. Second, the number of jets shows an increase with β. Because β is the first derivative of Coriolis parameter f, this might be an detailed implication about the positive relationship between rotation rate and jet numbers as in [Williams, G. P. et al., 1982].

4.1 PV Transportation

As is discussed above, our triggered convective parameterization regime produces MCs where in the domain, the stream function of a cyclonic regional minima point falls below the threshold value ψ_c. And the triggered PV forcing is centered on that point. These anti-cyclonic convective events move northern air parcels to the south, and southern ones to the north, which results in almost equal PV transport to south and north if not on a β plane. Because it evolves symmetrically. However, after MC transported northern air parcels around itself to the south, MC itself also tend to move southwards. So they "push" air parcels from the north further to the south, while southern parcels remain where they were. Normally air parcels north of the MC have PV larger than those in the south, so the comprehensive result is that MC move smaller PV from south to north and larger PV from north to south, while they cancel out the large northern PV they brought to the south with their own relatively negative PV values.

In view of eddy zonal momentum flux in the y direction, if we take zonal average over equation 3.2 and assume that partial derivative is commutative, we have:

$$\frac{\partial}{\partial t}\overline{q} = \frac{\partial^2}{\partial y^2}\overline{(v'u')}. \tag{4.1}$$

And we also consider eddy potential vorticity flux. We again take zonal average to

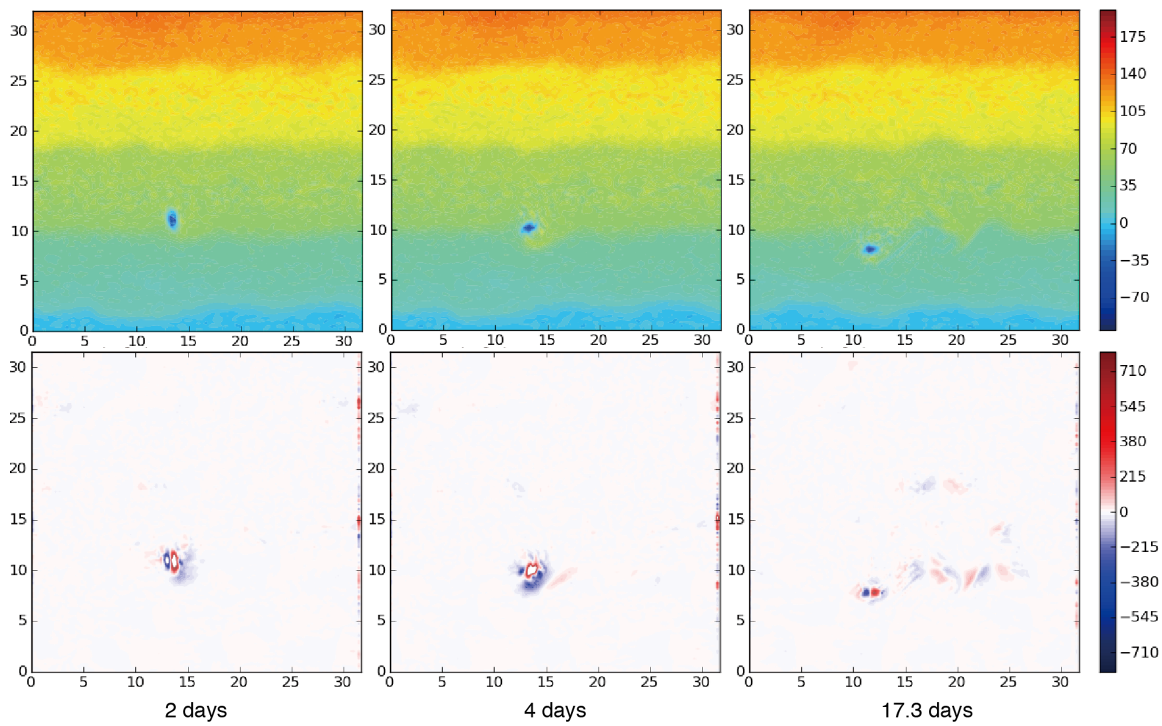

Figure 4-3: A typical process of MC transportation effect. Upper panels are PV fields of different stages in MC's lifetime; lower panels are PV transportation $q'v'$. 2 days after it is triggered, MC starts to move southwards. There starts to be strong surrounding negative PV transport on the right of MC and soft positive PV transport on the left. On the fourth day, surrounding negative PV transport starts to dominate while positive PV transport disappears; and positive PV transport within the MC is larger than negative PV transport. On day 17, MC's meridional movement slows down as the PV transport starts to be symmetric. Rossby waves are also generated in the northeast.

obtain:

$$\frac{\partial}{\partial t}\overline{q} = -\frac{\partial}{\partial y}\overline{(v'q')}. \tag{4.2}$$

The derivation of equation 4.1 and 4.2 is shown in Appendix A. From equation 4.1 we can see that the time derivative of zonal averaged PV is equal to second-order y derivative of zonal averaged eddy momentum transport, or negative first-order y derivative of eddy PV transport. If an eddy is generated in the domain, we take zonal average to show its PV transport effect: when $\partial\overline{(v'q')}/\partial y > 0$, the eddy tend to move PV from south to north, and when $\partial\overline{(v'q')}/\partial y < 0$, the eddy tend to move PV from north to south. If we look into the PV meridional transport $q'v'$ in one single PV event, as is shown in figure 4-2(c), we see that there is a blue band north and south of the MC track (shown as the black folded line), and red band around the MC. Here, red indicates positive PV meridional transport and blue indicates negative PV transport.

There are basically two aspects of PV transport (shown in figure 4-3): One is due to MC's movement to the south. When MC is generated with negative relative vorticity q', its left half has negative PV transport because $v' > 0$ and on its right half there is positive PV transport. Then when MC starts southward movement, v' of its left side diminishes, and v' of its right side strengthens. Therefore positive PV transport dominates, this is why red band surrounds MC in figure 4-2(c). The other is PV transport around the MC, being positive on the right margin and negative on the left margin of MC. And as MC starts to move south, the positive marginal transport on the left becomes negligible, and negative marginal transport on the right amplifies and becomes a semi-cycle around the MC. Taken zonal average, the first effect is larger than the second effect, so PV transport profile around MC is first negative, second positive, and then negative along y axis. Therefore, as MC moves from north to south crossing a certain latitude, $\partial\overline{(v'q')}/\partial y$ is positive and then negative, which means the zonal averaged PV along the way first decreases and then increases. This is Euler's view of PV transport.

4.2 PV Staircase

Due to our parameterization, MCs are always generated in the lowest parts in the domain, which is north of the jet band it's about to cross. And it is also a short distance from the steep part BC of PV staircase (illustrated in figure 4-4(a) and 4-4(b)). Whenever one MC is generated on a "staircase" AB, it moves across the joint part BC between the two staircases, and it usually disappears on the next staircase CD lower than AB. Once it is generated, it takes air parcels with large PV along to the south and they are replaced by air parcels from the staircase CD. As a result, a regional part of staircase AB is exchanged by part of CD, and this can be seen as a perturbation of Rossby wave on the staircase. The air parcels with large PV is mixed with MC itself on CD. Therefore, it appears that MC "takes" out PV on joint part BC while in fact there is a transportation and a mixing scheme. When taken zonal average, it appears that BC is pushed a bit northwards and becomes gentler as MC goes across. But it takes only a short time before BC is restored to its original slope.

When the MC, together with the air parcels it carries, goes further south, it mitigates because of mixing and dissipation, and so does the air parcels. In all, MC reduces the steep part of PV staircase by taking some of its air parcels away and mixing with them in the southern part of the domain. The obvious result is that when MC goes across the jet band, it "pushes" the jet to the north. There is generally considerably lots of MCs being generated in the domain, and as they goes southwards, crossing the jet bands to their south, they push every jet band in the domain northwards continuously, which appears that the jet bands migrate from south to north. The negative PV forcing of MCs must be balanced by positive radiation forcing S_r. More concretely, the radiation forcing drives PV all over the domain to increase uniformly, and in order to maintain conservation of PV, MCs are generated with negative PV, to balance the radiation forcing.

We assume that although MCs are the force that drives zonal jets to migrate, single convection has little effect on the PV staircase pattern. Thus zonal jet structure, also the PV staircase, stays the same after the model converges from initial stage to zonal

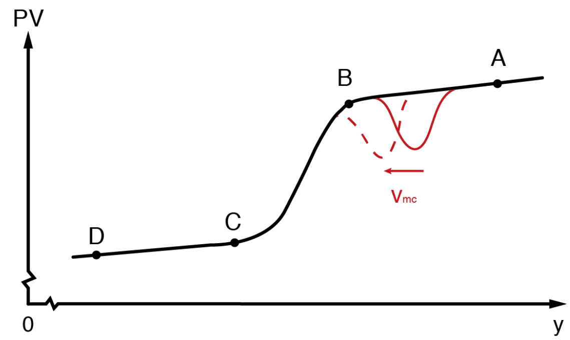

(a)

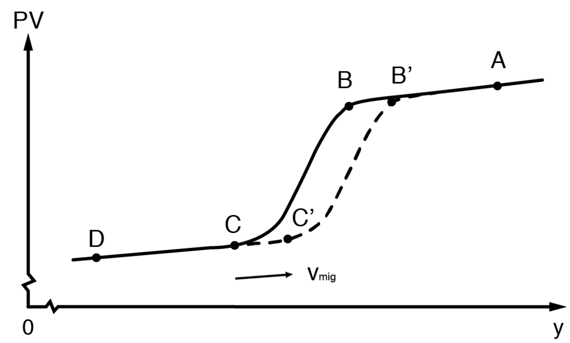

(b)

Figure 4-4: Diagram of PV staircase migration. Horizontal axis is y coordinate, and vertical axis is PV. Figure (a) shows when MC with negative PV is formed on staircase AB, it moves to the south with a velocity v_{mc}. Figure (b) shows that, after the PV transportation adjustment, the sloppiest part BC is pushed northwards to B'C', while staircase platforms AB and CD remain the same. Note that this is just a portion of the whole PV profile, and the effect of one-time MC migration is small, if not negligible.

stream stage (shown in figure 3-1 (a) and (d)), although they are pushed northwards intermittently by MCs. The PV staircase tends to increase because of radiation, and go northwards because of the MC transportation effect and staircase reconstruct scheme we mentioned above. As a result, the staircase ascends from lower left to upper right while remaining in the same periodic shape (figure 4-1).

4.3 Migration Speed

In this part we show that the migration speed's relationship with $S_r/beta$, and the fact that this relationship is also affected by β and L_d. The migration speed of each jet band is constant over the runtime. Therefore we choose one strong jet band emerging not too faraway from the southern boundary, and follow the point on it with fastest speed as a tracer. Then we take linear regression in t-y plane to get the migration speed.

According to the expression of PV, the basic slope of PV field should be β in y-pv plane (see also figure 5-1). From figure 4-5(a) we can see that migration speed is positively related with S_r and reversely related with β. The zonally averaged PV profile is constrained to a staircase-like shape in y-PV plane, which requires that he two schemes moving the staircase, radiative forcing, and MC forcing, has to balance with each other. In y-PV plane, the radiative forcing moves the staircase upwards while MC moves the staircase rightwards. The overall speed vector should be along the β slope, therefore, theoretically, the migration speed that we see in the physical world should be the projection of this vector on y axis. We then introduce $u_{mig} = S_r/\beta$ as a predictor of migration speed. However, the migration speed is not simply proportional to the reciprocal of β, and is also affected by β and Rossby wave number, which is determined by L_d (figure 4-5(b)).

For convenience, we separate each stair step in PV staircases into two parts, one is the "slope" connecting two levels of the stair, and the other is the "even platform" on each level. Also we divide the integrated speed of zonal averaged PV profile in y-PV plane into effective MC migration speed, which results from PV transportation

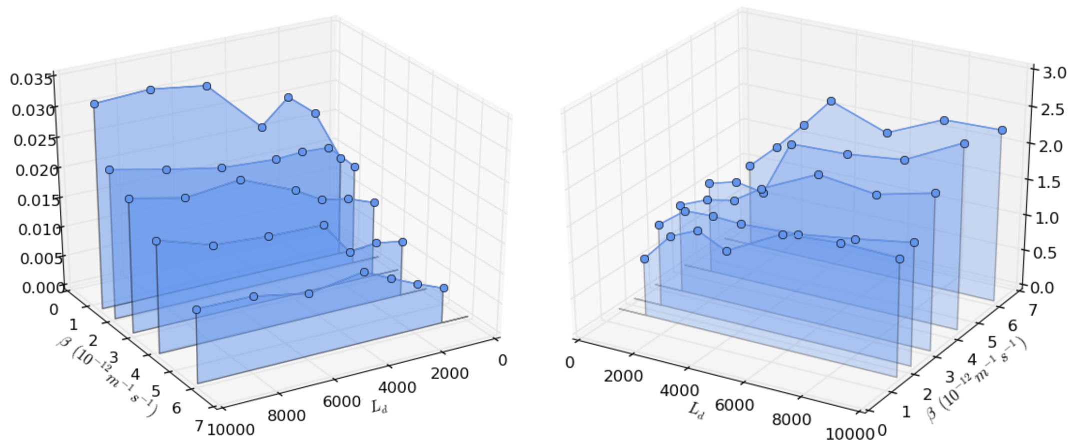

(a) (b)

Figure 4-5: The scatter plot of migration speed's dependence on L_d and β. The left figure (a) shows that migration speed is positively correlated with β and negatively correlated with L_d. On the other hand in (b), when divided by $u_{mig} = S_r/\beta$, the value migration speed over u_{mig} shows a reverse relationship with β (please note that (a) and (b) are presented from different angles to see more clearly), that is, the migration speed decreases more slowly than β^{-1}. And the migration speed is positively correlated with L_d as well.

of MCs, and effective radiation migration speed $S_r(s^{-2})$. We found two effects that strike influence on the deviation of actual migration speed from u_{mig}: (1) Multiple gradients of the even planes corresponding to different β selection; (2) the efficiency of interaction between small scale turbulence and large scale wave flow, determined by L_d and R_{mc}.

First, according to figure 4-6, the even part in each PV staircase profile is not horizontal, and is influenced by β, as larger β results in larger gradient of the even platform in y-PV plane. Therefore, when a single MC goes across a jet band, it will force the "slope" part of the staircase to move along the even plane's slope, causing the effective MC migration speed of the PV profile to be not in the horizontal right direction, but upper right direction along the platform slope. In this scheme, given the radiation effective migration speed S_r and even plane slope k', the actual migration speed is given by $u'_{mig} = S_r/(\beta - k')$, which is larger than u_{mig}. k' increases when β increases.

Second, migration speed has a positive correlation with Rossby Deformation Ra-

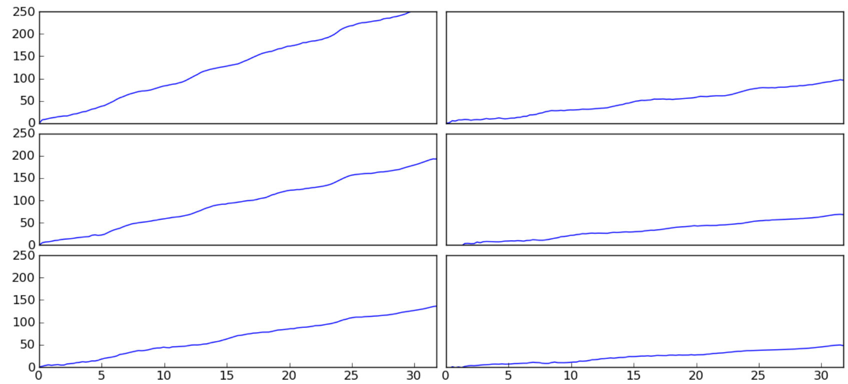

Figure 4-6: Zonally averaged PV gradient plot taken in 3.17 years after initiation. Each panel from top to bottom, left to right has β equaling to 8.52, 6.02, 4.26, 3.01, 2.13, $1.50 \times 10^{-12} m^{-1}s^{-1}$. When β increases, the gradient of each platform on the staircase increases, and so does the migration speed.

dius L_d, as is shown in figure C-2. In our experiments, when L_d is small, Rossby wave propagation speed is slower than when L_d is large, which makes zonal jets more constrained. And MCs seem to move more slowly to the south when L_d is small compared with large L_d values. We put forward a plausible explanation: in experiments of small L_d values, constrained Rossby wave patterns makes southward movement of MC difficult, so that one single MC has to spend more time in the jet band, where its marginal transportation of air parcels stalled because of mixing and dissipation. Therefore one MC is not capable to move as much northern PV to the south as when L_d is large. And as MC move slowly in y direction, they can't cross multiple jets and carry out more MC transportation effects before being dissipated into the domain. In other words, when L_d is large, MC carries out multiple migration effect so that the zonal jet migration speed is faster.

The fact that migration speed has to do with Rossby deformation radius has strong implications in geophysical fluid dynamics. In 2D geostrophic turbulence system, the zonal large scale structure is obtained by the inverse energy cascade that small scale injected energy tend to cascade into large scale, and the overlapping scale is expressed in the Rhines scale. However, it is not certain that how fast this cascade goes; in other words, how fast does vortexes merge into large zonal structure from their original scale? In our model, the Rossby wave on zonal jets differs significantly with the deformation radius L_d, where wavenumber increases with increasing L_d. We therefore introduce the wavelength scale, λ. In figure C-2 and figure 4-5(a), where R_{mc} is set to $1000km$, λ approaches R_{mc} as L_d increases. This lead to another explanation of the migration speed: when λ is near scale of the vortexes, it is easier for the vortex to transfer its energy into Rossby wave, and therefore it merges its negative PV value more easily into the slope part of PV staircase, which makes migration speed faster. If this was true, then the migration speed could be seen as an indicator for the interaction rate of MC and large scale zonal structure. On the other hand, the Rossby wavelength λ seems to be determined by L_d, but this awaits further experiments to justify. And of course this scale may as well connected with the Rhines scale.

Chapter 5

Jet Spacing

In our experiments, new jets emerge from the southern boundary while the old ones disappear on the northern boundary. The jets migrate in a periodic pattern with almost constant distances with each other, so that we can carry out statistic analysis on their average spacings. Our method is first take the smoothed zonal average of the zonal velocity in each time step, and calculate the distances between each peak and valley. Then average over all time steps to get the jet spacing value and standard deviation. The calculated value of jets pacing through all times at each L_d and β is shown in figure 5-1(a). Other parameters being equal, when L_d is large, simulated results have less jets, and therefore jet space becomes large.

As is mentioned in the introduction chapter, because of the anisotropy of β plane, the latitudinal scale of zonal jet does not agree with the meridional scale, and approaches infinity as evolvement proceeds. However, the meridional scale can be seen correlated with Rhines scale. The spacing of jets is also an indicator of meridional scale. We find that deformation radius L_d, and the total forcing strength of one single MC is related with jets spacing. For convenience, we introduce S_{int} which indicates the total PV forcing of one single MC. S_{int} is given by:

$$S_{int} = \pi R_{mc}^2 S_{mc} = \frac{\pi R_{mc}^2 T_{mc}}{12} S_{ampl} \tag{5.1}$$

Rhines scale is a good indicator of eddy-driven jets' spacing. Rhine's scale is given

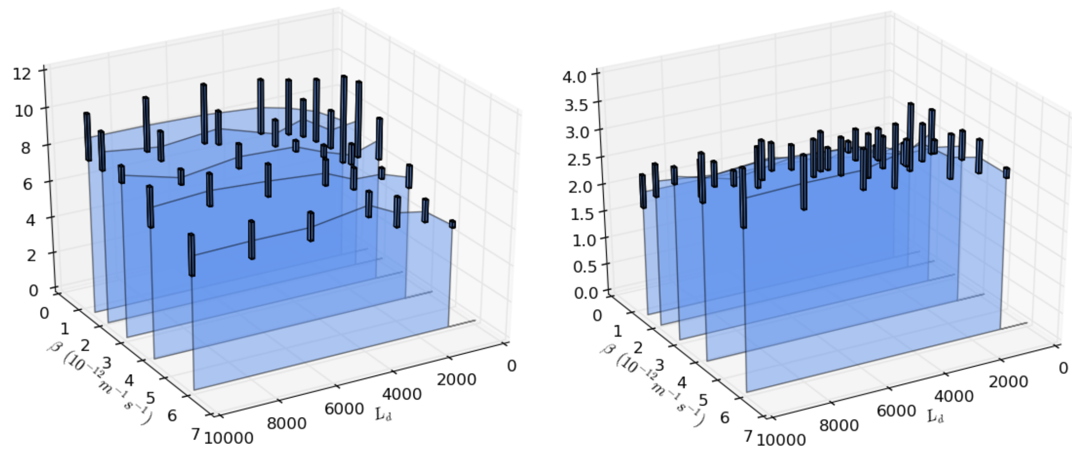

(a) (b)

Figure 5-1: (a) The calculated average peak-to-peak and valley-to-valley jet spacings in each experiments. The jet spacings show a slight decrease with increasing β and L_d. This behavior coincides with our estimation of the Rhines scale 5.3. (b) Actual jet spacings divided by Rhines scale. The obtained value does not show obvious trends with varying β and L_d, and is constrained between 2.0 and 3.5. The 3D bar represents the standard deviation of jet spacings.

by $L_R = \sqrt{\frac{U}{\beta}}$, where U refers to eddy velocity. We approximate U with equation 5.2:

$$U = \frac{R_{mc} T_{mc} S_{ampl}}{24} \left(\frac{1}{1 + \frac{R_{mc}^2}{8L_d^2}}\right). \tag{5.2}$$

Thus the Rhines scale is expressed as:

$$L_R = \left(\frac{S_{int}}{2\pi R_{mc} \beta} \left(\frac{1}{1 + \frac{R_{mc}^2}{8L_d^2}}\right) \right)^{1/2}. \tag{5.3}$$

In this equation, the jet spacing increases with decreasing L_d, and it is also negatively correlated with the moist convection radius R_{mc}, and positively correlated with the total PV forcing of one MC. The actual jet spacing acts similarly with L_R, (see figure 5-1(b)), in that jet spacing divided by L_R is constrained regardless of changing L_d and β. Therefore L_R is a good approximation of jet spacing.

Chapter 6

Conclusion and open questions

This thesis introduces the theoretical background of Jovian atmospheres and 2D geostrophic turbulence system on which our model is backed, and a brief description on our modelling frame. Then we demonstrated, explained and discussed in detail the decadal-scaled zonal jet migration phenomenon found in our prolonged integration time.

In our jovian 2D turbulence system, the radiative energy has to be balanced by moist convection. This can also be expressed by conservation of potential vorticity. Radiative forcing moves PV staircase upwards while MC push it northwards by transporting northern air parcels with large PV to the south. Therefore zonal jet migration is a must when radiation forcing and moist convection forcing are to be balanced by each other. According to this hypothesis, we introduced $u_{mig} = S_r/\beta$ and found that the actual migration speed is close to u_{mig}, which confirmed our hypothesis of PV transportation to explain dynamics of jet migration. We also explained the reason why actual migration speed deviates from u_{mig}: β and L_d.

The fact that L_d influences migration speed by controlling Rossby wavelengths could have implications toward hidden dynamics of interaction between moist convections and zonal jets. In our results, MCs cascade anisotropically to an infinite x scale and a certain y scale similar to the Rhines scale which is discussed in the previous literature, while showing a scale constant in x axis. The solution of Rossby waves is not constrained to a single wavelength in the x axis, but our results showed an scale λ controlled by L_d. Furthermore, this scale is determinative in the interaction between MC and zonal jet, in that the nearer the MC's scale R_{mc} is to λ, the easier MC gets torn apart by the Rossby wave, and the energy gets transferred from turbulence to wave form.

The above discussions leave some open questions for further investigation:

- What determines the particular Rossby wavelength in the model? It seems to be influenced by L_d, but it is also generated from MC transferring cascading from vortices to large-scale wave form. Thus there must be hidden dynamics that governs the behavior of MC's inverse cascade on a beta plane.

- Is the scale λ related with the Rhines scale in the latitudinal direction? Rhines scale can be interpreted as the jet spacing in the meridional direction, but there are not counterparts in the latitudinal direction. Rossby wavelengths, on the other hand, behaves quite similar to the Rhines scale as discussed in previous chapters. Therefore λ may quite likely be the candidate for Rhines scale in the latitudinal direction.
- Is there zonal jet migration on Jupiter? From our experiments, the zonal jet migrates in a scale of $10^{-2}m/s$, thus it may be unlikely that we observe this phenomenon from the available data we have. But whether the migration exists or not, investigating jets' behavior will be fruitful in the context of 2D turbulence systems.

Appendix A

Derivation of equation 4.1 & 4.2

We put zonal average over equation 3.2, and we have the following equation:

$$\frac{\partial}{\partial t}\overline{q} + \overline{J(\psi, \nabla^2\psi + \beta y)} = \overline{S_r} + \overline{S_{mc}} \tag{A.1}$$

where $\nu\nabla^2\zeta$ is averaged to zero because of periodical boundary condition in the x direction and $\zeta = 0$ on boundaries in the y direction. As for each term in A.1, $\overline{J(\psi, \nabla^2\psi)}$ is given by:

$$\begin{aligned}
\overline{J(\psi, \nabla^2\psi)} &= -\overline{\frac{\partial}{\partial x}(\frac{\partial}{\partial y}\nabla^2\psi)} + \overline{\frac{\partial}{\partial y}(\frac{\partial}{\partial x}\nabla^2\psi)} \\
&= \overline{\frac{\partial}{\partial y}(\frac{\partial}{\partial x}\nabla^2\psi)} \\
&= \overline{\frac{\partial}{\partial y}(\frac{\partial\psi}{\partial x}\frac{\partial^2\psi}{\partial y^2})} \\
&= -\overline{\frac{\partial}{\partial y}(u'\frac{\partial v'}{\partial y})} \\
&= -\overline{\frac{\partial^2}{\partial y^2}(u'v')} + \overline{\frac{\partial}{\partial y}(u'\frac{\partial v'}{\partial y})}.
\end{aligned} \tag{A.2}$$

And $\overline{\frac{\partial}{\partial y}(u'\frac{\partial v'}{\partial y})} = -\frac{\partial}{\partial y}\overline{\frac{\partial\psi}{\partial y}\frac{\partial}{\partial x}(\frac{\partial\psi}{\partial y})} = 0$ if we assume the y derivative and zonal average is commutable. And we are talking about eddy momentum flux, whose time scale is small compared with the adequate time for S_r to have a large effect, and around eddy, there is usually no other eddies around, so the terms $\overline{S_r}$ and $\overline{S_{mc}}$ all equal to zero. thus we have:

$$\frac{\partial}{\partial t}\overline{q} = \frac{\partial^2}{\partial y^2}\overline{(v'u')}. \tag{A.3}$$

As for the eddy PV(potential vorticity) flux, we have from equation 3.2:

$$\frac{\partial}{\partial t}\overline{q} + \overline{\frac{\partial}{\partial y}(q\frac{\partial \psi}{\partial x})} - \overline{\frac{\partial}{\partial x}(q\frac{\partial \psi}{\partial y})} = 0. \tag{A.4}$$

where $\overline{\frac{\partial}{\partial x}(q\frac{\partial \psi}{\partial y})} = 0$ and $\overline{\frac{\partial}{\partial y}(q\frac{\partial \psi}{\partial x})} = \frac{\partial}{\partial y}\overline{(qv)} = \frac{\partial}{\partial y}\overline{(q'v')}$, because $\overline{v} = \frac{\overline{\partial \psi}}{\partial x} = 0$ for the boundary conditions, and $\overline{v'} = 0$. Therefore we have:

$$\frac{\partial}{\partial t}\overline{q} = -\frac{\partial}{\partial y}\overline{(v'q')}. \tag{A.5}$$

Appendix B

Approximation of U, in equation 5.2

We rewrite equation 3.1 as follows:

$$\frac{d}{dt}(\nabla^2\psi - k_d^2\psi + \beta y) = S(r,t) + S_r + \nu\nabla^2\zeta \tag{B.1}$$

In this equation, S_r and $\nu\nabla^2\zeta$ has only long-term effect, and βy is dominant only on magnitude of the whole domain. Thus these three terms are neglected when discussing eddy velocities. Integrating both sides for one convection's time, we have:

$$(\nabla^2\psi - k_d^2\psi)_{convection} = S_{ampl}(1 - \frac{r^2}{R_{mc}^2}) \tag{B.2}$$

We solve this equation when $k_d \sim 0$ and $k_d^2\psi \gg \nabla^2\psi$ corresponding to L_d being relatively large and small compared with zonal jet structures. When $k_d \sim 0$, equation B.2 becomes:

$$\frac{1}{r}\frac{\partial}{\partial r}(r\frac{\partial\psi}{\partial r})\psi = S_{ampl}(1 - \frac{r^2}{R_{mc}^2}) \tag{B.3}$$

The solution is $U = \frac{\partial\psi}{\partial r} = \frac{S_{ampl}R_{mc}T_{mc}}{24}$, and when $k_d^2\psi \gg \nabla^2\psi$, equation B.2 becomes:

$$-k_d^2\psi = S_{ampl}(1 - \frac{r^2}{R_{mc}^2}) \tag{B.4}$$

U is then solved as $U = S_{ampl}/(3k_d^2 R_{mc})$. Interpolate between these two solutions gives equation 5.2.

Appendix C

Parameter exploration

C.1 Experiment description

We have done several series of cases to inspect the impacts of parameterization factors, including deformation radius L_d, β, convection radius R_{mc}, convection active time T_{mc}, and convection amplitude S_{ampl}. The relationship of migration speed and spacing with L_d, β and S_r is shown in figure C-1 and C-2.

In order to test our hypothesis that we should keep integrated vorticity source S_{mc} to maintain similar pattern, we varied parameters but kept S_{mc} the same all the time. Figure C-3 shows the cases where we keep S_{ampl} the same and vary L_d and R_{mc} together with T_{mc}, when figure C-4 shows cases when we keep T_{mc} the same and vary L_d and R_{mc} together with S_{ampl}. The parameters were chosen according to table C.1 and table C.2.

$R_{mc}(km)$	$T_{mc}(days)$	$S_{ampl}(10^{-12}s^{-2})$
500	7.87	3750
1000	1.97	3750
2000	0.49	3750
4000	0.12	3750

Table C.1: We set S_{ampl} constant in this series of experiments, and vary L_d from $500 \times 10^3 km$ to $16000 \times 10^3 km$ by factor of 2 for each set of R_{mc}, T_{mc} and S_{ampl}

$R_{mc}(km)$	$T_{mc}(days)$	$S_{ampl}(10^{-12}s^{-2})$
250	1.97	60000
500	1.97	15000
1000	1.97	3750
2000	1.97	937.5
4000	1.97	234.4

Table C.2: We set T_{mc} constant in this series of experiments, and vary L_d from $1000 \times 10^3 km$ to $8000 \times 10^3 km$ by factor of 2 for each set of R_{mc}, T_{mc} and S_{ampl}

C.2 Figures

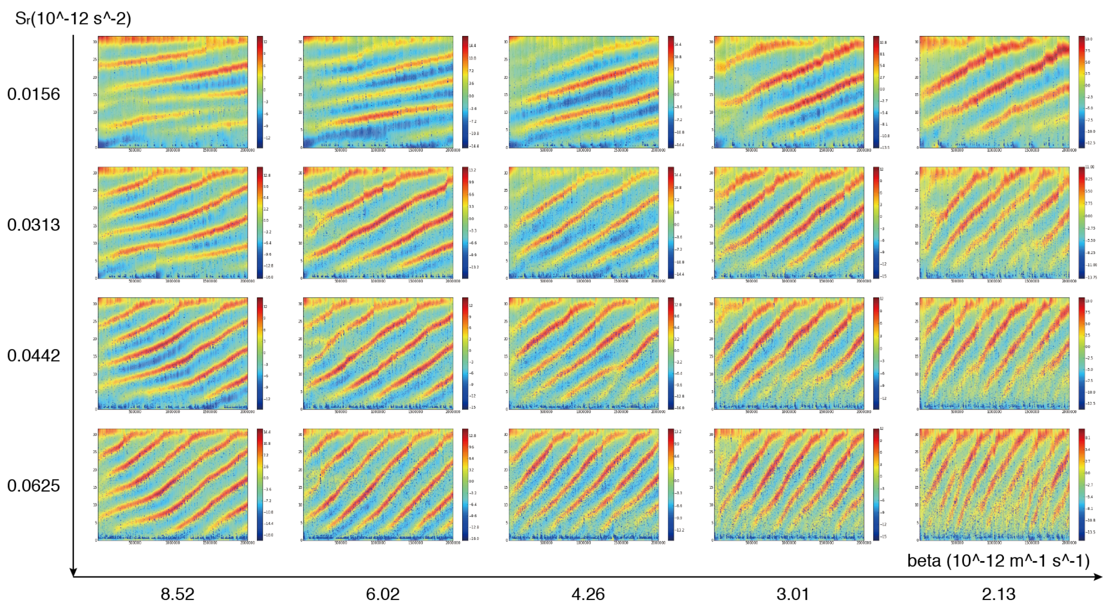

Figure C-1: A series of experiments finding out the impacts of radiation forcing S_r and β. The vertical axes indicates decreasing order of S_r, while the horizontal axes indicates different β of an increasing order. It is clear that increasing S_r or decreasing β will all result in larger migration speed. At the same time, jet spacing does not appear to be affected by these two parameters.

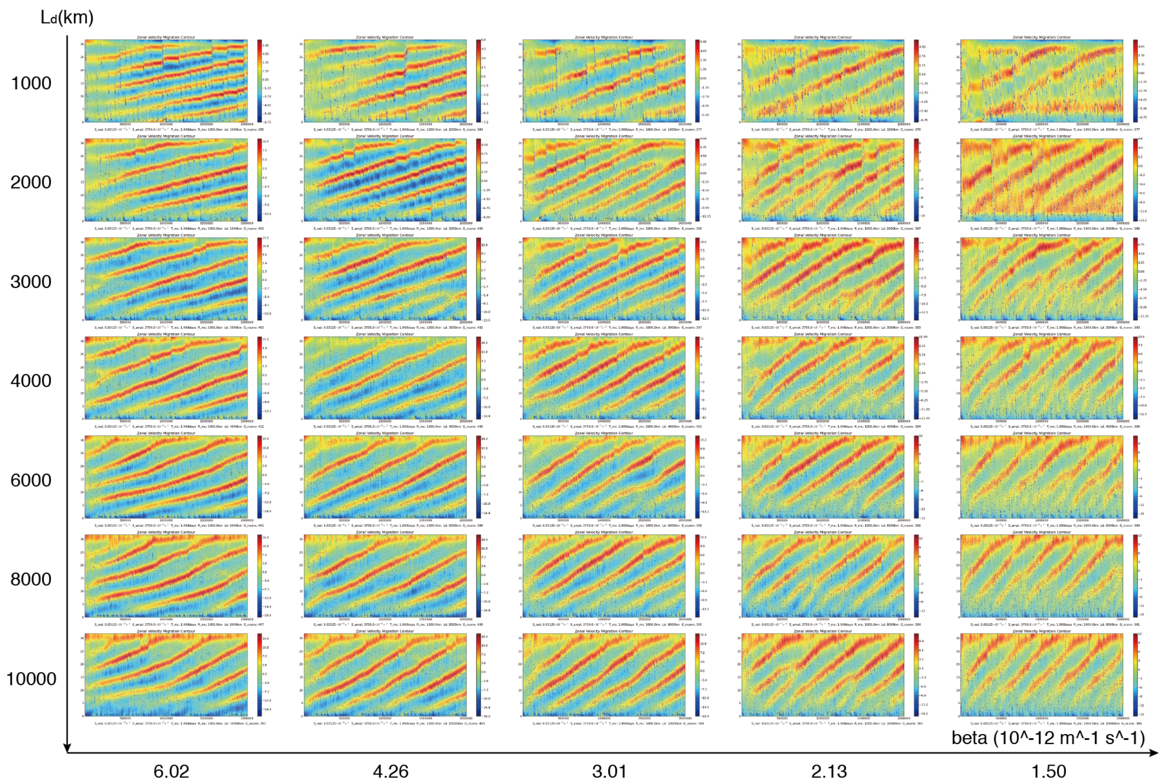

Figure C-2: Another series of experiments when we vary L_d in the vertical axes and β in the horizontal direction. Although it is certain that β affects the migration speed, there is a positive correlation between L_d and migration speed. On the other hand, the jet spacing increases with decreasing β and increasing L_d, which corresponds to the Rhines scale, which is approximated via equation 5.2.

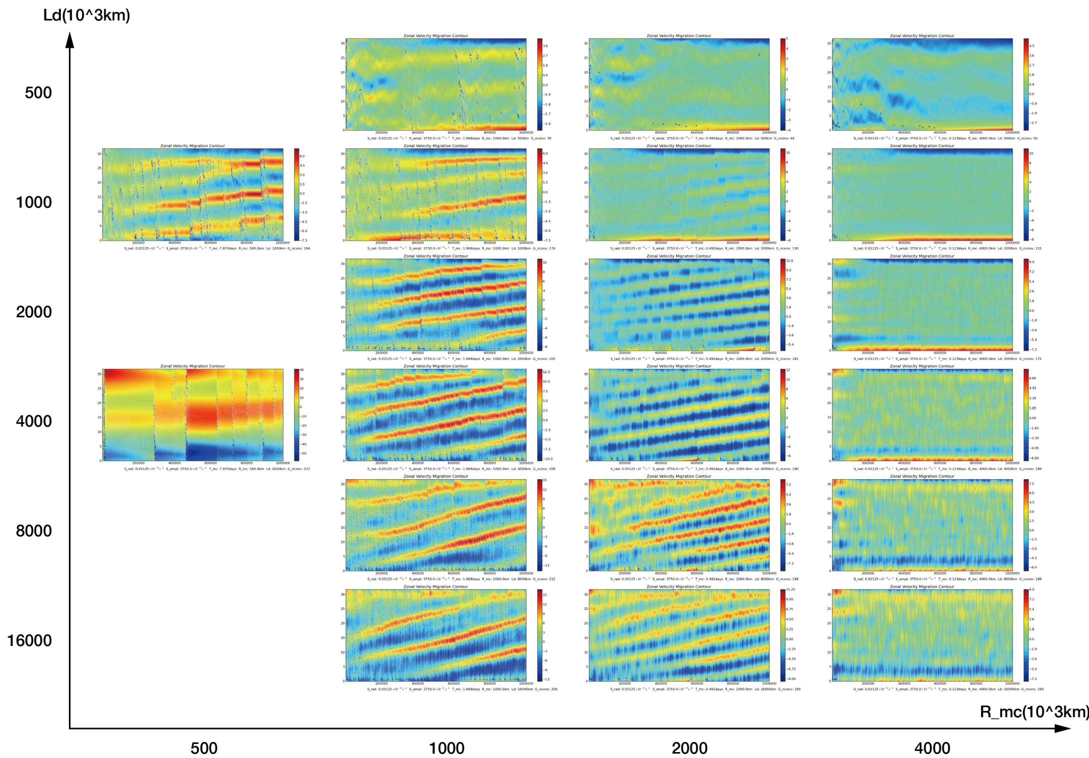

Figure C-3: A third series of experiments finding out the impacts of deformation radius L_d and the radius of convective events R_{mc}. The vertical axes indicates decreasing order of L_d, while the horizontal axes indicates different R_{mc} of an increasing order. When varying R_{mc}, we keep integrated convection source S_{int} the same by varying T_{mc} at the same time. The blank portion when $R_{mc} = 500km$ is when the model "blows up". We can see in the second and third column that as R_{mc} increases, jets' spacing becomes narrower, which agrees with our prediction of Rhines scale 5.3.

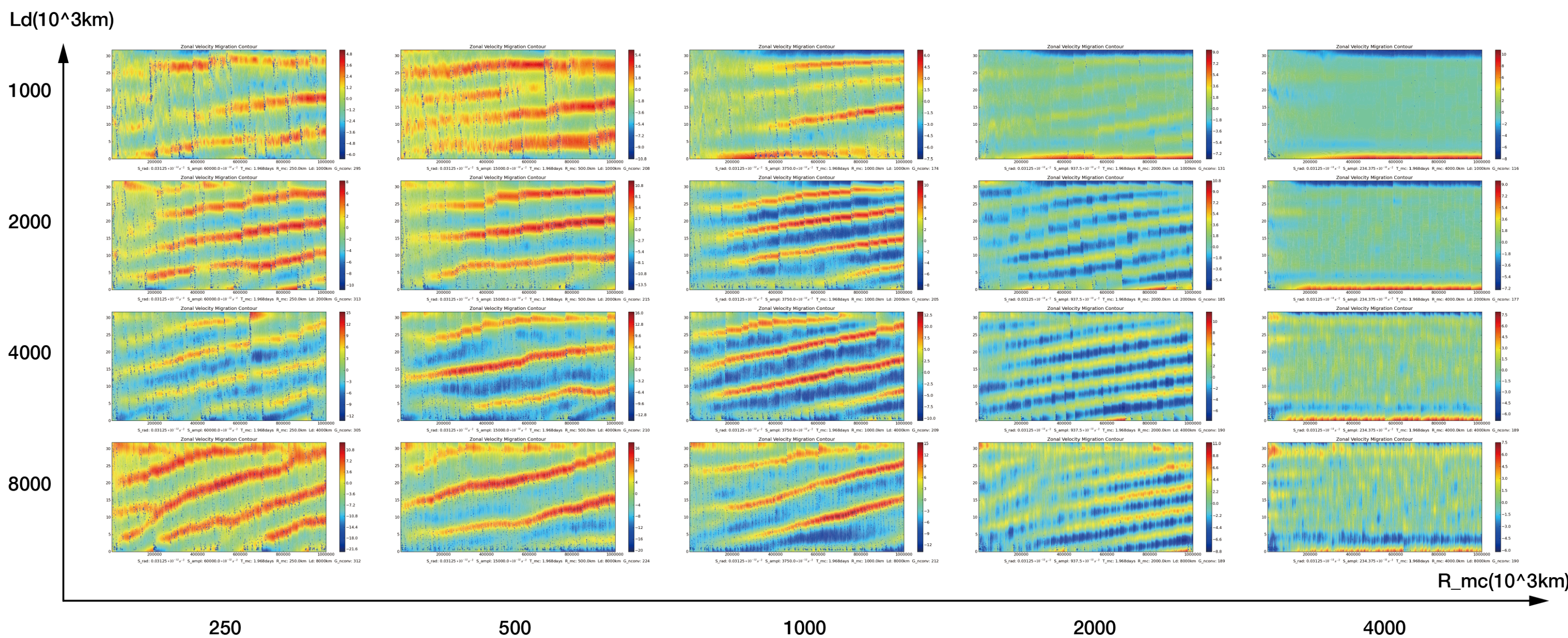

Figure C-4: Another series of experiments when we vary Ld in the y axes and R_{mc} in the x axis. Apart from figure C-3, We keep integrated vortex source S_{int} by varying S_{ampl} at the same time, so that T_{mc} is the same in all of these cases. As we kept T_{mc} the same, the model's output seems more stable because convective forcing is distributed more evenly over time.

Bibliography

[Rivera, M. K., 2000] Rivera, M. K., 2000 The Inverse Energy Cascade of Two-Dimensional Turbulence. *arXiv*, http://arxiv.org/pdf/physics/0103050.pdf

[Williams, G., 1978] Williams, G. P., 1978 Planetary Circulations: 1. Barotropic Representation of Jovian and Terrestrial Turbulence. *J. Atmos. Sci.*, 35, 1399-1426.

[Schombert, J., 2004] Schombert, J., 2004 Primary Atmospheres. *Astronomy 121: Lecture 14 Terrestrial Planet Atmospheres*

[Arakawa, A., 1966] Arakawa, A., 1966 Computational Design for Long-Term Numerical Integration of the Equations of Fluid Motion: Two-Dimensional Incompressible Flow. Part I. *J. Comput. Phys.*, 1, 119–143.

[Chemke, R. et al., 2015] Chemke, R., Kaspi Y., 2015. Poleward migration of eddy-driven jets. *J. Adv. Model. Earth Syst.*, 07, doi:10.1002/2015MS000481.

[Dyudina, U.A. et al., 2004] Dyudina, U.A., Del Genio, A.D., Ingersoll, A.P., Porco, C.C., West, R.A., Vasavada, A.R., Barbara, J.M., 2004. Lightning on Jupiter observed in the H_α line by the Cassini imaging science subsystem. *Icarus*, 172, 24-36.

[Li, L. et al., 2005] Li, L., Ingersoll, A., and Huang, X. (2005) Interaction of moist convection with zonal jets on Jupiter and Saturn. *Icarus*, 180, 113-123.

[Little, B. et al., 1999] Little, B., Anger, C.D., Ingersoll, A.P., Vasavada, A.R., Senske, D.A., Breneman, H.H., Borucki, W.J., 1999. Galileo images of lightning on Jupiter. *Icarus*, 142, 306-323.

[Press, W. H. et al., 1986] Press, W. H., Teukolsky, S. A., Vetterling, W. T., Flannery B. P., 1986 Numerical Recipes in Fortran *Cambridge University Press*

[Rhines, P. B., 1975] Rhines, P. B., 1975 Waves and turbulence on a beta-plane. *J. Fluid Mech.*, 69, 417-443.

[Scott, R. K. et al., 2007] Scott, R. K. and Polvani, L. M., (2007) Forced-Dissipative Shallow-Water Turbulence on the Sphere and the Atmospheric Circulation of the Giant Planets. *J. Atmos. Sci.*, 64, 3185-3176.

[Showman, A. P., 2006] Showman, A. P. (2006) Numerical Simulations of Forced Shallow-Water Turbulence: Effects of Moist Convection on the Large-Scale Circulation of Jupiter and Saturn. *J. Atmos. Sci.*, 64, 3132-3157.

[Taylor, F. W., 2010] Taylor, F. W., 2010 Planetary Atmospheres. *Oxford University Press*, 261 pp.

[Vallis, G. K. et al., 1993] Vallis, G. K., Maltrud M. E., 1993 Generation of Mean Flows and Jets on a Beta Plane and over Topography *J. Phys. Oceanogr.*, 23, 1346-1362.

[Vallis, G. K., 2006] Vallis, G. K., 2006 Atmospheric and Oceanic Fluid Dynamics. *Cambridge University Press*

[Williams, G. P. et al., 1982] Williams, G. P., Holloway, G. L., 1982. The range and unity of planetary circulations. *Nature*, 297(5864), 295-299.

[Williams, G. P., 2002] Williams, G. P., 2002. Jovian Dynamics. Part III: Multiple, Migrating, and Equatorial Jets. *J. Atmos. Sci.*, 60, 1270-1296.